Chapter 17
Theranostics: In Vivo

Viktorija Herceg, Norbert Lange and Eric Allémann

Abstract Theranostics is a portmanteau of thera(py) and (diag)nostics. It is an interdisciplinary field of research that unites pharmaceutical technology, chemistry, imaging, and medicine with the purpose of creating a single drug delivery system able to diagnose, treat, and monitor disease. In this chapter, the reader will be presented with an overview of the state-of-the-art developments in theranostics in which clinically relevant imaging modalities are combined with polymers, lipid-based systems, inorganic assemblies, antibody conjugates, and gene delivery vehicles. Here, special emphasis will be placed on the systems tested in vivo.

Keywords Theranostics · In vivo · Polymer systems · Lipid-based systems · Inorganic assemblies · Gene therapy

1 Introduction

In order to overcome the pitfalls of conventional xenobiotics, such as high toxicity, adverse effects, multiple-drug resistance (MDR), low drug diffusion into the target sites, and rapid clearance from the body, a rational approach to designing nanoconstructs with multiple functions was developed. In this context, nanomedicine can be defined as the application of nanotechnology for in vitro and in vivo medical purposes. The advent of nanomedicine began in the mid-1990s when liposomal doxorubicin formulations (Doxil® and Daunoxome®) gained market approval as anticancer therapeutics. This was directly followed by paclitaxel-loaded

V. Herceg · N. Lange · E. Allémann (✉)
School of Pharmaceutical Sciences, University of Geneva, University of Lausanne, Rue Michel-Servet 1, 1211 Geneva 4, Switzerland
e-mail: Eric.Allemann@unige.ch

V. Herceg
e-mail: Viktorija.Herceg@unige.ch

N. Lange
e-mail: Norbert.Lange@unige.ch

C. Vauthier and G. Ponchel (eds.), *Polymer Nanoparticles for Nanomedicines*,
DOI 10.1007/978-3-319-41421-8_17

Table 1 Classification of theranostics

Therapeutic approach	Treatment mechanism	Imaging modality	References
Conventional treatment	Active pharmacological ingredient	OI/MRI/PET/SPECT	Agulla et al. (2014a), Alexiou et al. (2000), de Smet et al. (2011), Grange et al. (2010), Kaida et al. (2010), Lammers et al. (2009), Lee et al. (2013), Nurunnabi et al. (2010), Ponce et al. (2007), Quan et al. (2011), Ranjan et al. (2012), Topete et al. (2014), Wu et al. (2014), Yu et al. (2008)
Photothermal therapy	Heat	OI/MRI/US	Bardhan et al. (2010), Charan et al. (2012), Cheng et al. (2012, Gao et al. (2014), O'Neal et al. (2004), Peng et al. (2011)
PDT	PS/light/O_2	OI	Topete et al. (2014), Gabriel et al. (2009), Jang et al. (2011), Zeisser-Labouebe et al. (2009)
Gene therapy	Oligonucleotides	OI/MRI/PET/SPECT	Wang et al. (2012), Wang et al. (2013)
Radioimmunotherapy	X-rays	OI/PET/SPECT	Bander et al. (2005), Stillebroer et al. (2013), Tagawa et al. (2013)

nanoparticles (Abraxane®) (Modery-Pawlowski and Gupta 2014). Most importantly, due to their intrinsic multimodal nature, nanoparticulate drug delivery systems have opened new doors toward the development of theranostic agents. In such systems, a therapeutic and an imaging agent are contained in the same delivery vehicle. Theranostics provides the real-time monitoring of a given treatment in a noninvasive manner. It grants patients a better therapeutic outcome by maximizing the safety profiles. Depending on the design and characteristics of theranostic systems, they can be classified as treatments with an active pharmaceutical ingredient, photothermal therapy, photodynamic therapy (PDT), gene therapy, radioimmunotherapy, or combinations of the abovementioned strategies (Table 1). In this sense, supramolecular nanoconstructs as drug/imaging agent carriers provide potential advantages over small molecules, such as improved bioavailability, decreased systemic toxicity, and reduced severity of adverse effects (Hoste et al. 2004). Moreover, the use of nanocarriers provides a way to efficiently deliver poorly water-soluble drugs and enables the incorporation of multiple imaging tags in a single platform. Most importantly, the use of polymer nanosystems allows the encapsulation of multiple agents in a confined space even when the therapeutic and imaging agents are distinct chemical entities. Taken together, these advantages make polymer systems good candidates for theranostic purposes. A polymer-based nanotheranostic system is composed of a polymer, therapeutic agent, and an imaging agent. Targeting ligands may be added to these structures to enhance the treatment specificity (Fig. 1).

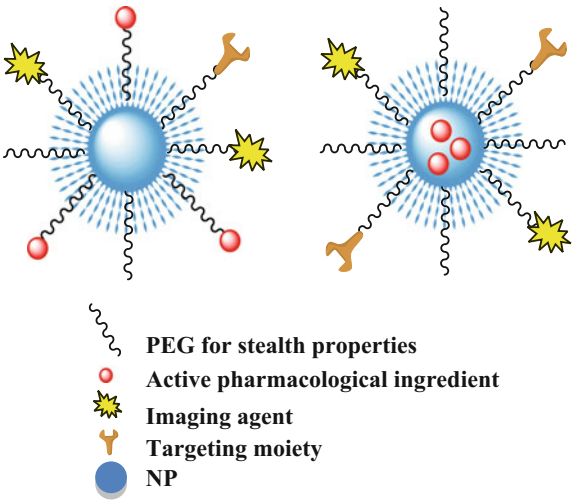

Fig. 1 Schematic representation of polymer-based nanotheranostic systems

There are two ways of delivering nanoparticles (NPs) to the desired site of action: passive and active targeting. The former depends on the enhanced permeability and retention (EPR) effect, first reported by Matsumura and Maeda (1986). EPR is typically described in tumor biology and is characterized by the combination of the leaky architecture of angiogenic blood vessels with fenestrations between adjacent endothelial cells and a poor lymphatic drainage inside the tissue (Hagendoorn et al. 2006). As a result, NPs are able to better extravasate and accumulate inside solid tumors. Numerous factors, including anatomical and microscopic defects in the tumor vasculature, the presence of molecular factors in the extracellular matrix, such as vascular endothelial growth factor (VEGF), bradykinin, prostaglandins, nitric oxide, peroxynitrite, and proteolytic activity, can have an impact on the EPR effect (Iyer et al. 2006). Improvement of the theranostic agents may be achieved by adding active targeting moieties.

Active targeting strategies can be classified into the following categories (Fig. 2):

1. attaching ligands onto the surface of NPs, such as antibodies, antibody fragments, affibodies, peptides, nucleic acids, and others (vitamins and carbohydrates), that bind to the receptors of the targeted cells (Peer et al. 2007; Accardo et al. 2013);
2. using of tissue-specific physiological triggers, such as enzymatically cleavable (Gabriel et al. 2009) or pH-responsive linkers; and
3. physical targeting by externally applied magnetic fields, ultrasound, light (McCarthy et al. 2010), or heat (Ganta et al. 2008).

Recently published literature on theranostics have reported on systems that were not necessarily yet tested in vivo (Chen et al. 2011; Mura and Couvreur 2012; Xie et al. 2010; Janib et al. 2010; Svenson 2013; Luk and Zhang 2014). The purpose of the present chapter is to address examples of theranostic systems with an emphasis

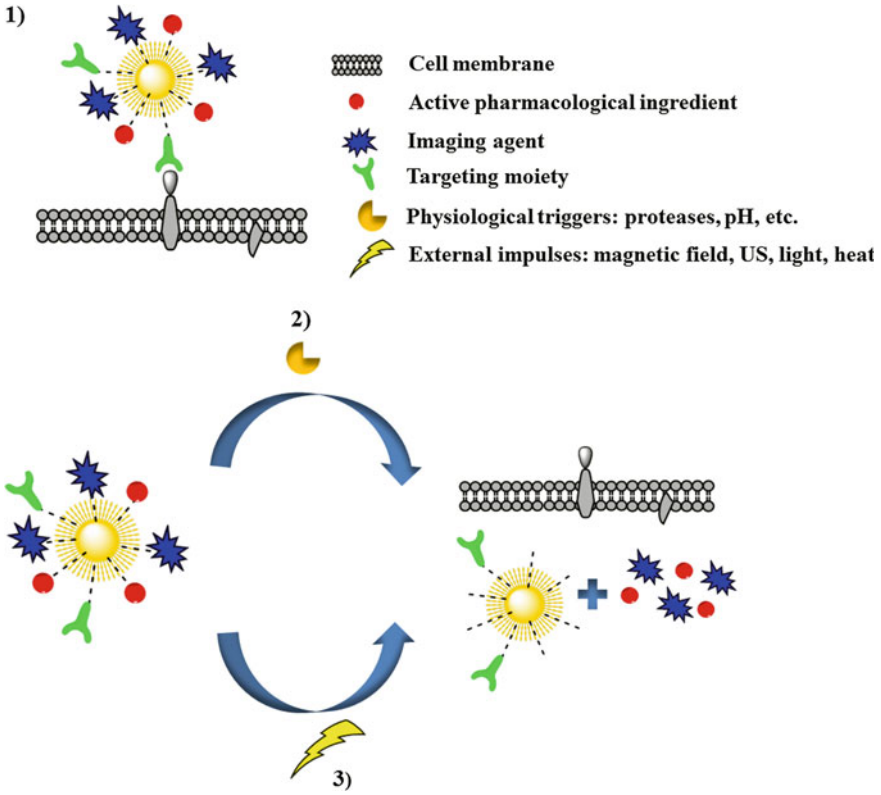

Fig. 2 Active targeting strategies. *1* Attachment of specific ligands to the nanoparticles. *2* Use of tissue-specific triggers such enzymatic digestion or pH-responsive linkers. *3* Physical targeting by external impulses

on their in vivo assessments for both therapeutic and diagnostic functions. We will focus our attention on the imaging modalities used in clinical practice in combination with a wide range of NPs including polymer conjugates and complexes, liposomes, micelles, inorganic assemblies, theranostic NPs used for gene delivery, and antibody conjugates for radioimmunotherapy. The review will be useful to understand which functionalities may be incorporated into polymer-based NPs to design tools for theranostic application.

2 Imaging Modalities

Various imaging modalities are available in clinical practice for disease diagnosis and treatment monitoring. In this chapter we will cover examples of ultrasound (US), optical imaging, X-ray imaging computed tomography (CT), magnetic

Table 2 Commonly used imaging modalities

Imaging modality	Agent used	Spatial resolution	Advantages	Disadvantages
US	Microbubbles	50 μm	High sensitivity, no radiation, quantitative	Low depth penetration
Optical imaging	Fluorochromes	1–5 mm	High sensitivity, no radiation	Low depth penetration
CT	Iodine or barium-based agents	50 μm	High spatial resolution, speed	Requires high atomic mass contrast agents that have to be administered at molar concentration
MRI	Gd chelates, Mn, iron oxide nanoparticles	10–100 μm	High resolution, no radiation, unlimited tissue penetration, quantitative	Long imaging time
PET	^{18}F, ^{15}O, ^{13}N, ^{11}C,	1–2 mm	High sensitivity, unlimited tissue penetration, quantitative	Radiation, limited spatial resolution
SPECT	^{99}mTc, ^{123}I, ^{131}I, ^{111}In	1–2 mm	High sensitivity, unlimited tissue penetration, quantitative	Radiation, limited spatial resolution

resonance imaging (MRI), and radionuclide-based imaging such as positron emission tomography (PET) and single-photon emission computed tomography (SPECT). Table 2 summarizes the main characteristics of the commonly used clinical imaging modalities. The successful implementation of clinical imaging for therapeutic monitoring relies on high signal-to-background ratios (SBRs) to reliably discriminate the diseased and surrounding healthy tissues (Frangioni 2008). With the current state of nanotechnology, all agents of the aforementioned imaging techniques can now be incorporated into nanoconstructs for theranostic purposes.

2.1 Ultrasound

Ultrasound imaging is broadly available, noninvasive, relatively easy to implement, and is one of the most employed diagnostic techniques for the examination of soft tissues in clinical practice. An US transducer placed on the skin of a patient emits sound waves that penetrate the body. US images are subsequently created from backscattered waves coming from different tissue structures. For further contrast enhancement and differentiation between healthy and diseased tissues, microbubbles

with unique acoustic properties can be used. Microbubbles are typically 1 to 4 μm spheres of perfluorocarbons surrounded by phospholipids, proteins, or polymers (Dijkmans et al. 2004; Kiessling et al. 2012) and are designed to circulate within blood vessels but not extravasate. US imaging has a high enough sensitivity allowing for the detection of a single microbubble (Deckers and Moonen 2010). Although microbubbles have been reported as a promising platform for drug delivery (Eisenbrey et al. 2009, 2010a, b; Cochran et al. 2011), their gas core and the single phospholipid outer layer of bubbles is unsuitable for the efficient encapsulation of therapeutic molecules. Another limitation for their application in theranostics is that US-mediated drug release causes signal loss upon microbubble disruption (Deckers and Moonen 2010). Therefore, subsequent administrations of microbubbles would be required for treatment monitoring. Although interesting, the concept of using two separate formulations for active drug delivery and for therapeutic monitoring is beyond the scope of this chapter and will not be further discussed.

2.2 *Optical Imaging*

Optical imaging uses photons emitted from different sources to visualize living tissues. Optical imaging can be further categorized as fluorescence imaging, photoacoustic imaging, and absorption-based imaging. Due to its high sensitivity, fluorescence imaging is the primary optical image technique used in clinical practice. However, photoacoustic imaging and diffusion-based techniques have recently gained the attention of clinicians (Choe et al. 2009; O'Sullivan et al. 2013; Leproux et al. 2013). Unlike MRI, SPECT, PET, or CT, optical imaging permits the monitoring of the treatment during surgical interventions (Keereweer et al. 2011; van Driel et al. 2014; van Dam et al. 2011; Heath et al. 2012). Optical imaging is safe for patients, relatively simple to use, and can be repeated frequently. The major limitation for optical imaging is the low penetration of light into deeply seated sites due to light scattering in the tissue. Furthermore, if improperly selected, the fluorescent signal of the contrast agent may interfere with tissue autofluorescence. Today, most of the optical imaging studies are directed toward near-infrared (NIR) markers, which offer better results for in vivo diagnoses and treatment monitoring. The advantages of NIR imaging include the increased penetration of light into tissues and an increased SBR due to a low tissue autofluorescence at these wavelengths (Keereweer et al. 2011; Adams et al. 2007). Currently, there are numerous studies describing NIR-guided open surgery, laparoscopy, thoracoscopy, and robot-assisted surgery (Vahrmeijer et al. 2013; Keereweer et al. 2013). Agents that are routinely employed in intraoperative fluorescence imaging are methylene blue, indocyanine green (ICG), and 5-aminolevulinic acid (5-ALA) (Vahrmeijer et al. 2013). Intravital microscopy and whole-body photonic imaging are techniques in which optical fluorescence imaging is employed in vivo (Mulder et al. 2007).

Photoacoustic imaging (PAI) is a newly developed technique that provides high-resolution images in tissues beyond the limit of optical diffusion. PAI uses

chromophores, which induce a thermoelastic expansion in the tissue when excited. This generates an acoustic pressure waves that can be measured by an ultrasound transducer (Ng et al. 2014; Huynh et al. 2014).

NIR diffuse optical tomography and spectroscopy are two rapidly developing fields for disease detection and diagnosis. These absorption-based imaging techniques employ low-power NIR light to measure wavelength-dependent optical absorption coefficients in tissues. The results obtained by this measurement provide direct information about physiological properties, such as blood dynamics, total hemoglobin concentration, oxygen saturation, and water and lipid concentrations (Choe et al. 2009; O'Sullivan et al. 2013; Leproux et al. 2013; Konecky et al. 2009).

2.3 X-Ray Computed Tomography

X-ray CT enables 3D reconstructions based on the attenuation of an X-ray beam that passes through the body. The generated CT images provide anatomical information due to differences in the X-ray absorption of different tissues (Janib et al. 2010). The benefits of using CT are its high spatial resolution, availability, and speed. To improve contrast, iodinated contrast agents are routinely used for imaging vasculature (i.e., angiography) (Hasebroock and Serkova 2009) and barium-based agents for gastrointestinal investigations. However, one major drawback for the creation of usable nanotheranostics for CT imaging is that a suitable contrast agent must have a high atomic mass and be delivered at very high doses (Frangioni 2008).

2.4 Magnetic Resonance Imaging

Magnetic resonance imaging is a highly versatile, noninvasive diagnostic technique with high temporal and spatial resolutions. However, the major drawbacks of this imaging modality include its low sensitivity and high cost (Terreno et al. 2010). MRI signals are detected from water protons in tissues when the body is placed in a magnetic field generated by an MR scanner. Hence, the contrast of an MR image is determined by the proton density in tissues and their relaxation times following a radio frequency pulse. Different paramagnetic, superparamagnetic, and ferromagnetic contrast agents are used to enhance MRI signals by shortening the relaxation time of water in the tissues. T1 agents, also called positive or bright contrast agents, such as gadolinium (Gd) and manganese (Mn) chelates, increase the signal intensity. T2 contrast agents decrease the signal intensity and are accordingly referred to as negative or dark contrast agents (Weishaupt et al. 2006; Davies et al. 2013). T2 contrast agents are mainly iron oxide-based particles. Overall, the most frequently used contrast agent is Gd (Davies et al. 2013; Caravan 2006). However, free Gd is highly neurotoxic and thus, is required to be tightly chelated in molecules such as tetraazacyclododecane tetraacetic acid (DOTA) (Davies et al. 2013). To overcome

the low sensitivity of MRI, high doses of contrast agents need to be delivered. For this purpose, various NPs have been developed that encapsulate high payloads of Gd to amplify the signal contrast and to optimize the relaxivity of the imaging agent itself (Terreno et al. 2010, 2012). However, the use of Gd-based contrast agents may lead to severe adverse effects, such as nephrogenic systemic fibrosis (Hasebroock and Serkova 2009).

2.5 Radionuclide-Based Imaging, PET, and SPECT

The basis for both PET imaging and SPECT imaging is the emission of gamma γ-rays from exogenously administered radioactive tracers. In PET imaging, the radionuclide undergoes positron emission decay. Then, the emitted positron loses its kinetic energy, and by encountering an electron, an annihilation process occurs. The produced pairs of γ-photons move in opposite directions and are detected by PET cameras to create an image (Fig. 3). ^{18}F, ^{15}O, ^{13}N, and ^{11}C are radionuclides commonly used for PET imaging (Massoud and Gambhir 2003), and ^{99m}Tc, ^{123}I, ^{131}I, and ^{111}In are commonly used for SPECT imaging (Peng et al. 2011) (Table 3). Because of an increased glucose metabolism, the glucose mimetic, 2-deoxy-2-[^{18}F] fluoro-D-glucose (^{18}FDG), is readily taken up by the brain or by cancerous cells and is used in various diagnostic procedures. Compared to PET agents, which have to be administered shortly after their synthesis because of their short half-lives, radionuclides used in SPECT are easier to prepare and have longer half-lives, which makes them suitable for treatment monitoring for hours or days after the

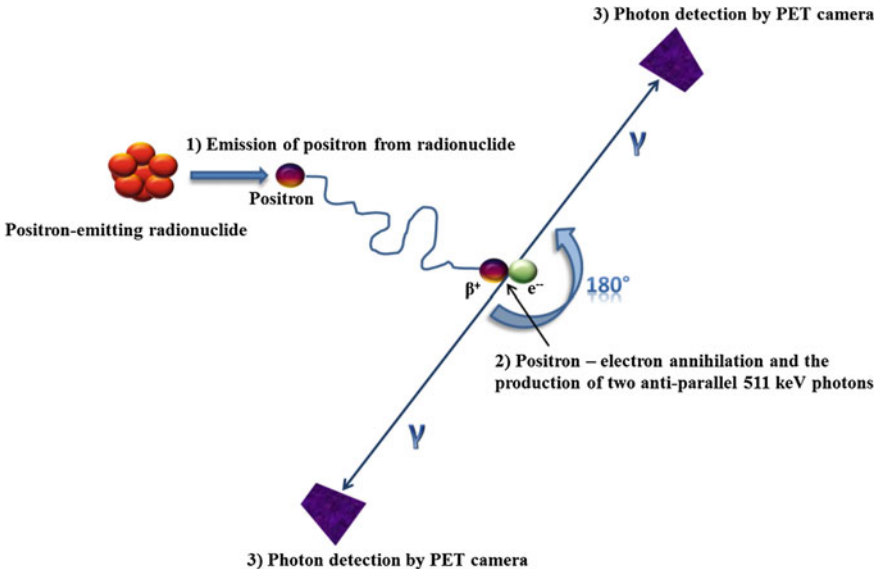

Fig. 3 Principle of PET imaging process

Table 3 Commonly used radionuclides for PET and SPECT imaging

Type of imaging	Radionuclide	Half-life
PET	^{18}F	110 min
	^{15}O	2 min
	^{13}N	10 min
	^{11}C	20 min
SPECT	^{99m}Tc	6 h
	^{123}I	13 h
	^{131}I	8 days
	^{111}In	2.8 days

administration of the imaging agent (Rahmim and Zaidi 2008; Beer and Schwaiger 2008). Additionally, in SPECT imaging, it is possible to simultaneously use several radionuclides (Janib et al. 2010). Both modalities possess unlimited depth penetration, but have limited spatial resolution. An advantage of PET over SPECT imaging is its two to three orders of magnitude higher sensitivity (Rahmim and Zaidi 2008). Radionuclide-based imaging for theranostic purposes remains quite limited not only because of the short half-lives of most isotopes, but also because of the strict radioactive safety requirements.

3 Theranostic Nanosystems

3.1 Polymer Systems

In the mid-1970s, H. Ringsdorf proposed an ideal model of polymer prodrugs. An early version of minimal theranostic system is described in his model, which consisted of a biodegradable polymer backbone as a carrier onto which spacers for drug conjugation, imaging agents, and targeting moieties were attached (Fig. 4) (Ringsdorf 1975). Several polymers have already been successfully tested in the development of polymer therapeutics, including vinyl polymers such as poly(*N*-(2-hydroxypropyl) methacrylamide) (PHPMAm) (Kopecek and Kopeckova 2010; Duncan 2003); poly(styrene-*co*-maleic acid/anhydride) (PSMA) (Maeda 2001); synthetic poly(α-amino acids), such as poly(L-lysine) and poly(L-glutamic acid); polysaccharides, such as dextran and chitosan (Liu et al. 2008); and proteins, such as human serum albumin (HSA) (Hoste et al. 2004; Miele et al. 2009).

Polymer conjugates include rationally designed macromolecular drugs, polymer–drug, and polymer–protein conjugates (Duncan 2003; Khandare and Minko 2006). The chemical assembly depends on the properties of the polymer carrier, the targeting moiety, and the drug and imaging agent to be attached (Veronese et al. 2005; Furgeson et al. 2006). Due to the huge variation of physical–chemical properties of the individual building blocks, the preparation of the final product can be challenging. The choice between homopolymers, graft, or block polymers for the conjugation of the drug and imaging agents and the chemical yield is dependent on

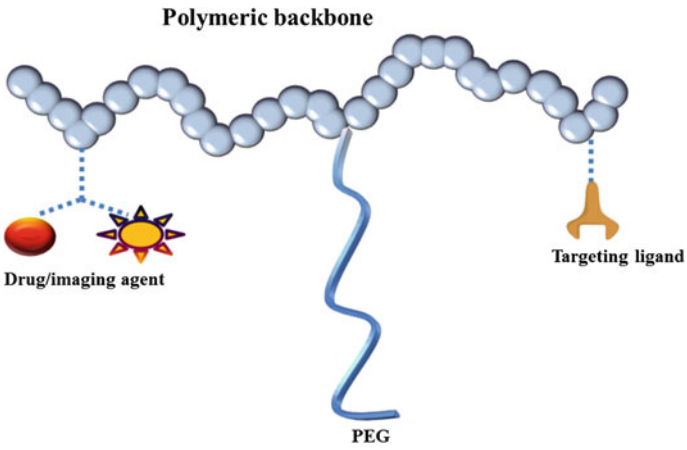

Fig. 4 Model of a polymer prodrug. A polymer backbone serves as a carrier for drugs, imaging agents, and targeting moieties. A hydrophilic unit, such as PEG, enhances the solubility and provides stealth properties

the chemical nature, molecular weight, steric hindrance, and reactivity of the polymer and the drug and imaging agents (Khandare and Minko 2006). One of the main requirements in polymer systems is a good stability between the carrier and its payload under physiological conditions. However, the carrier and payload should be rapidly cleaved once the target site is reached (Veronese et al. 2005). By using enzymatically cleavable or pH-responsive linkers, this can be exploited as an active targeting strategy for the controlled release of therapeutic agents in the region of interest. For instance, it is known that upregulated proteolysis is found in cancer, cardiovascular, neurodegenerative, and inflammatory diseases among others (Gabriel et al. 2011). In cancer, the breakdown of the extracellular matrix and subsequent extravasation is largely facilitated by tumor-associated cells that are abundantly expressing several proteases. These proteases can be identified as a hallmark of neoplastic growth. In this case, the most prominent proteases are matrix metalloproteinases, cysteine proteinases, plasminogen activators, and cathepsin D (Gabriel et al. 2011). This enzymatic machinery can be used for the activation of prodrugs and imaging agents (Gabriel et al. 2011; Harris et al. 2008). Another means to trigger drug release is by exploiting changes in the pH of the tumor environment. This has been shown to be successful in solid tumors, which produce large amounts of lactic acid due to anaerobic glycolysis and acidify interstitial fluid. Thus, suitable target pH values for the release of the attached agent can be tuned to the physiological values at the targeted location, i.e., the extracellular domain of the cancerous cells or their intracellular compartments, such as endosomes or lysosomes.

Polymer chemistry research for biomedical purposes has focused on the synthesis of nontoxic and biodegradable polymers. Examples of such polymers in polymer prodrugs include, but are not limited to, poly(lactide) (PLA) (Kulkarni et al. 1971) and poly(lactide-*co*-glycolide) (PLGA) (Danhier et al. 2012). Because

of its stability in systemic circulation and its nontoxicity and low immunogenicity, HPMAm polymer is also frequently used for both complexations (Vasey et al. 1999) and conjugations of drugs and imaging agents (Hoste et al. 2004; Janib et al. 2010; Kopecek and Kopeckova 2010). Lammers et al. (2008) reported a series of experiments with a supramolecular assembly in which cytostatic drugs doxorubicin (DOX), gemcitabine (GEM), or both (Lammers et al. 2009) were conjugated via a lysosomally cleavable peptide linker to the polymer backbone of an HPMAm copolymer. First, PHPMAm-bound DOX or GEM were tested in combination with radiotherapy (Lammers et al. 2008). To monitor the in vivo biodistribution, the HPMAm copolymer was labeled with Gd and imaged by MRI. As expected, the MRI images showed an enhanced accumulation of the construct in tumors over time. However, because there was no therapeutic agent attached, these constructs cannot be classified as theranostics. In the subsequent study, an HPMAm polymer–drug conjugate was designed, carrying 6.4 wt% GEM and 5.7 wt% DOX. Tyrosinamide units were incorporated into the copolymer to allow radiolabeling with ^{131}I. The in vivo study carried out in the Dunning AT1 tumor model confirmed the simultaneous delivery of both drugs to the tumors (Lammers et al. 2009). It would have been interesting to see the potential of the aforementioned PHPMAm construct labeled with Gd for theranostic applications. Both findings shed new light on the simultaneous multimodal approaches of cancer treatment and its future theranostics implementation.

PDT and photodiagnosis (PD) are other exciting fields that have been introduced in clinical practice with high efficacies for both diagnostic and therapeutic purposes. Three factors govern the PDT mechanism: a photosensitizer (PhotoS), light, and molecular oxygen in the target tissues (Lange 2003). Irradiation with light excites the administered photosensitizer, which converts molecular oxygen into toxic singlet oxygen molecules and reactive oxygen species (ROS) (Gabriel et al. 2011). Moreover, upon light activation, the emitted fluorescence from the PhotoS can serve as a diagnostic tool. Most conventional PhotoSs are generally hydrophobic and prone to aggregation in aqueous environments. Therefore, their administration in pharmaceutically acceptable formulations is impeded. Furthermore, their bioavailability is often very low without an appropriate formulation. To overcome these obstacles, PSs have been conjugated to peptides, proteins, carbohydrates, and polymers or loaded into micelles, dendrimers, liposomes, or other types of polymer NPs (Sibani et al. 2008). One such example is the encapsulation of a potent natural PhotoS hypericin into polymer PLA NPs, as reported by Zeisser-Labouebe et al. (2006). Hypericin-loaded NPs obtained by nanoprecipitation were tested in vivo on an ovarian cancer xenograft in Fischer rats F-344. Fluorescence endoscopy and tissue analyses showed the selective accumulation of hypericin in ovarian micrometastases when the NPs were used in comparison with the free drug (Zeisser-Labouebe et al. 2009). In addition to cancer, rheumatoid arthritis (RA) is another disease in which PDT has been successfully tested in vivo. RA is a chronic autoimmune disease characterized by the inflammation of the synovial tissues of joints, tendon sheets, and bursae that lead to the progressive destruction of the articular cartilage. Thrombin is a serine protease of the coagulation cascade converting fibrinogen into fibrin. In RA patients, the proteolytic activity of thrombin has been found to be upregulated. Gabriel et al. (2009)

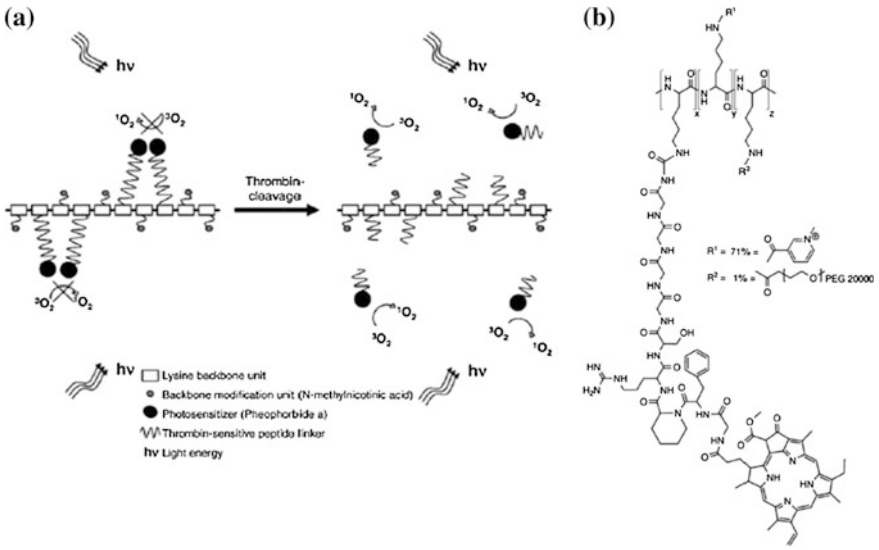

Fig. 5 **a** Schematic representation of protease-mediated activation of thrombin-sensitive polymer photosensitizer prodrug (T-PhotoS). Coupled to the poly-lysine backbone, PhotoSs remained quenched, but upon thrombin cleavage of the peptide linker, they were freed and could be light activated, which resulted in fluorescence emission and ROS production; **b** schematic representation of T-PhotoS. Adapted from Gabriel et al. (2009)

developed a thrombin-sensitive polymer photosensitizer prodrug (T-PhotoS) for the photodynamic eradication of the hyperplastic synovium in RA. In their prodrug, multiple PhotoS units were tethered to a polymer (poly-lysine) backbone via thrombin-cleavable peptide linkers. Moreover, the polymer backbone was modified with single high molecular weight PEG (20 kDa) (Fig. 5). The close proximity of the PhotoSs attached to the copolymer resulted in the inactivation of the fluorescence signal and the photodynamic activity due to self-quenching. The in situ activation of T-PhotoS was demonstrated in vitro and in vivo using a collagen-induced arthritis mice model. T-PhotoS was administered intravenously and the fluorescence intensity in inflamed joints was observed by whole animal fluorescence imaging. A fluorescence increase over time was observed to occur selectively in arthritic joints, whereas the fluorescence emissions in non-arthritic paws remained close to baseline. The fluorescence rapidly increased during the first 8-h post administration and then reached a plateau. Furthermore, the fluorescence intensity after i.v. injection of T-PhotoS at a dose of 1 mg/kg pheophorbide equivalence correlated with established clinical scores (Fig. 6). A similar approach was followed for the targeting of urokinase-like plasminogen activator (uPA), which is involved in the progression of prostate cancer, and was tested in vitro and in vivo (Zuluaga et al. 2012, 2013). The selectivity of the corresponding PhotoS in PC-3 tumors was confirmed by the colocalization of bioluminescence and fluorescence imaging. Furthermore, uPA-mediated PDT resulted in the cure or partial remission of tumors in the PDT group only.

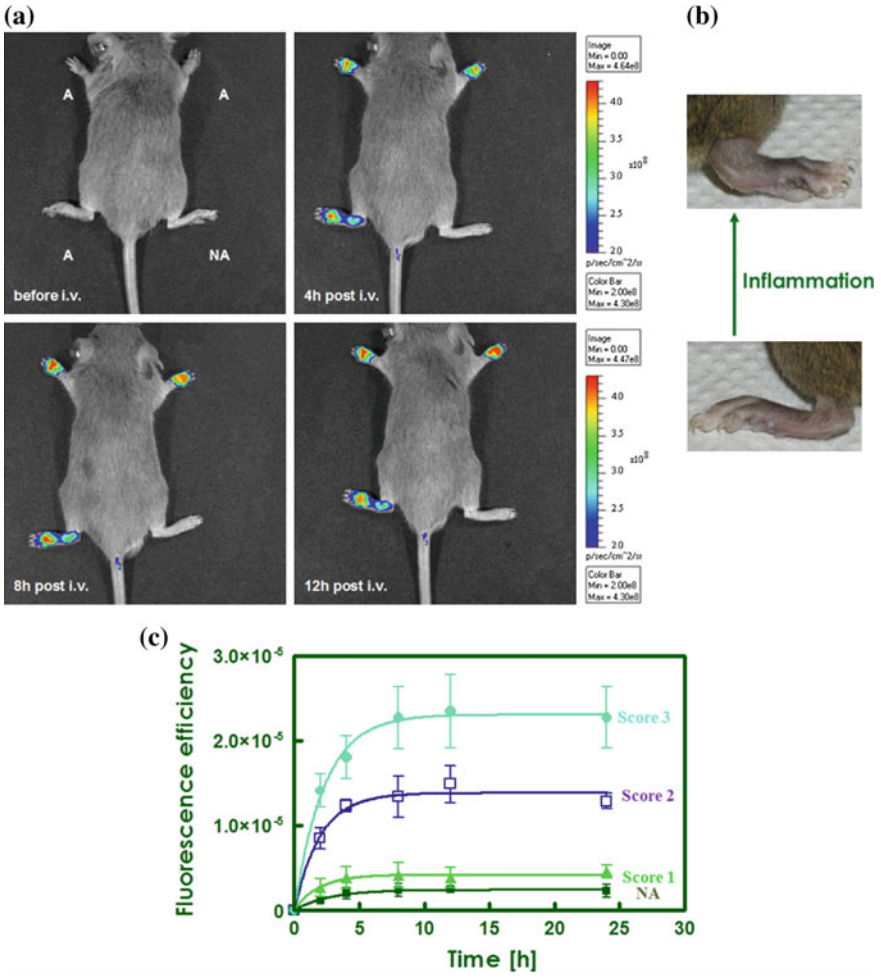

Fig. 6 **a** Quantitative in vivo fluorescence images acquired before, 4, 8, and 12 h post i.v. injection of T-PhotoS at a dose of 1 mg/kg pheophorbide equivalents. Selective fluorescence increase can be seen in the arthritic paws (*A*), but not in the non-arthritic paws (*NA*). **b** Image of the normal versus inflamed joints in mice. **c** Fluorescence time profiles show a rapid increase of fluorescence in arthritic paws during the first 8 h after T-PhotoS administration and subsequent plateaus. Here, fluorescence enhancement was related to the clinical score of inflammation. Adapted from Gabriel et al. (2009)

Photothermal therapy is another promising approach to treat diseases that circumvent the adverse side effects caused by conventional drugs. It is based on the optical properties of certain molecules or NPs that dissipate energy as heat upon the absorption of light. A double targeting strategy explored in a theranostic supramolecular photothermal agent between an NIR dye squaraine (SQ) and bovine serum albumin (BSA) indicated promising results for both tumor ablation and noninvasive imaging. An SQ–BSA construct was compared to another carrying

folate as a targeting moiety (SQ–BSA–FA). Folate is a critical nutrient for DNA synthesis, methylation, and repair and its receptor is often overexpressed in rapidly dividing cells, such as in the case of cancers (Gao et al. 2014; van Dam et al. 2011). SQ–BSA–FA was found to be preferentially retained in tumors due to passive targeting and active retention. Extravasation of administered formulation is by its nature always passive, but the following retention process is active due to the interaction between the receptor and targeting ligand. Photothermal treatment with both products resulted in the inhibition of tumor growth of up to 32 % for SQ–BSA and up to 78 % for SQ–BSA–FA. The benefits of active targeting were confirmed both by NIR imaging during the treatment and later by histology (Gao et al. 2014).

Photothermal cancer treatment was also proven possible by using PEGylated nanoconstructs based on a poly(3,4-ethylenedioxythiophene):poly(4-styrenesulfonate) (PEDOT:PSS) polymer mixture covered with poly(allylamine hydrochloride) (PAH) and poly(acrylic acid) (PAA). The PEG termini of PEDOT:PSS-PEG were labeled with a fluorescent dye Cy5 to follow the in vivo behavior in 4T1 murine breast-cancer-bearing mice. Fluorescent imaging was performed at 1, 4, 8, 24, and 48 h after NP administration. The increasing fluorescence intensity with time in tumors confirmed the uptake of NP by the EPR effect. To investigate the therapeutic potential of these agents, mice were divided into four groups. The first group received PEDOT:PSS-PEG at a dose of 1 mg/ml and was exposed to an 808-nm laser at a power density of 0.5 W/cm^2 for 5 min 48 h post-injection. The other three groups are untreated mice, laser only, and PEDOT:PSS-PEG without laser irradiation served as controls. The mice injected with PEDOT:PSS-PEG and exposed to the laser showed a complete eradication of tumors after only 1 day of treatment. No noticeable toxicity was reported (Cheng et al. 2012). These findings confirmed the potential of a photothermal tumor ablation approach for theranostic purposes.

4 Lipid-Based Nanosystems

4.1 Liposomes

Liposomes are aqueous vesicles surrounded by a phospholipid bilayer. As drug delivery systems they have been exploited mainly with sizes ranging between 50 and 200 nm (Patil and Jadhav 2014). Depending on the preparation and purification techniques, liposomes may vary in structure from unilammellar vesicles to multi-layered formulations (Patil and Jadhav 2014). Because they are composed of a hydrophilic core and a hydrophobic lipid bilayer, liposomes are well-suited for the delivery of both hydrophilic and hydrophobic compounds. This makes them perfect candidates for theranostic delivery systems. Specific ligands can be easily attached on the liposomal surface to achieve active targeting. Various labels for diagnostic imaging can also be conjugated to the surfaces (Torchilin 2005). Although liposomes are one of the most widely used delivery systems, their main drawback is their rapid opsonization and uptake by the cells of the reticuloendothelial system (RES) in the

liver and the spleen. One of the most employed strategies to avoid uptake and clearance by the RES is the incorporation of hydrophilic PEG chains onto the surface of liposomes (Harris and Chess 2003; Torchilin et al. 1994). Due to the association of water molecules, PEG acts as a shield against enzymatic degradation and opsonization by plasma proteins. Overall, the attachment of PEG improves the in vivo pharmacokinetics (Chen et al. 2004), prolongs the circulation time of particles, and gives liposomes "stealth" properties (Harris and Chess 2003; Torchilin et al. 1994).

Liposomes have been designed to target integrins, a family of heterodimeric cell surface receptors involved in cell adhesion, motility, growth, and survival. One of the mostly targeted proteins of this family is the $\alpha_v\beta_3$ overexpressed on the vascular endothelium and significantly involved in angiogenesis. Peptides containing the arginine–glycine–aspartic acid (RGD) motif are often used for the specific targeting of the $\alpha_v\beta_3$ integrin on angiogenic endothelial cells (Beer and Schwaiger 2008; Chen et al. 2004; Mittra et al. 2011; Teesalu et al. 2013). Another target for anti-angiogenic treatment is neural cell adhesion molecules (NCAMs). NCAM is a protein that belongs to the superfamily of immunoglobulins (Ig). Its role in cell–cell interactions is found to be important in tumor-associated angiogenesis (Bussolati et al. 2006) and is a valuable target for high-affinity NCAM-binding peptides (Geninatti Crich et al. 2006). Grange et al. (2010) prepared NCAM-binding peptide (C3d)-coated PEG liposomes encapsulated with DOX and a lipophilic (Gd)-DOTA–monamide (DOTAMA) derivative. In vivo studies with these liposomes were carried out in a model of Kaposi's sarcoma in SCID mice. The results indicated a more efficient tumor regression and a lower toxicity when using NCAM-targeted liposomes compared with untargeted counterparts. Interestingly, the MRI signals were higher for the untargeted liposomes. This was attributed to the efficient internalization of targeted paramagnetic vesicles into the cells that limited the relaxation enhancement due to the reduced exchange of water molecules across the intracellular compartments.

Theranostic liposomes were developed by Agulla et al. (2014a) for the treatment of stroke. Their formulation encapsulated citicoline and contained rhodamine for fluorescence and Gd ions for MR imaging. Active targeting was achieved by conjugating the protein HSP72, a biomarker of the peri-infarct region. Both the diagnostic and the therapeutic potential of the liposomal formulation were assessed on an in vivo rat model of ischemic stroke. The MRI T1 mapping of the brain of ischemic rats was performed 1 day before and 1, 3, and 7 days post-intervention. Promising results were obtained with respect to the targeting potential of the vectorized liposomes in the delineation and the follow-up of the peri-infarct tissue. To further evaluate the therapeutic potential of anti-HSP72 liposomes, a permanent focal cerebral ischemia was performed in six groups of Sprague-Dawley rats. The results showed the highest therapeutic effect in rats intravenously injected with HSP72-targeting liposomes encapsulated with citicoline at $t = 45$ min and 6, 12, 24, and 30 h post-surgery. Lesion volumes were significantly smaller in comparison with the controls at day 1, day 2, and day 7 post-surgery, and compared with citicoline encapsulated in nontargeted liposomes (Agulla et al. 2014a).

An active targeting with liposomes is also possible by taking advantage of acidic pH changes in subcellular compartments. A pH-sensitive liposome can be achieved

by modifying their lipid composition, incorporating pH-sensitive polymers, or a combination thereof. This type of liposome prevents the premature release of an active principle or an oligonucleotide during gene therapy (Torchilin 2005). The release of the cargo from pH-sensitive liposomes is triggered by the acidic endosomal environment as was demonstrated by a kinetic model of the cellular uptake and release of MRI agents (Delli Castelli et al. 2010).

One of the most promising theranostic agents and certainly the most advanced in terms of clinical development is the thermosensitive DOX-loaded paramagnetic liposome designed for MRI (Langereis et al. 2013). These liposomes not only circumvent the undesirable side effects of DOX, but also enable the assessment of therapeutic efficacy. In thermosensitive liposomes (TSLs), the cytotoxic drug, and the imaging agent are entrapped within the aqueous lumen at normal body temperatures and are released in cancerous tissue upon the application of local hyperthermia (de Smet et al. 2011). It was demonstrated that hyperthermic conditions enabled the efficient extravasation of small liposomes (Kong et al. 2000; Kong et al. 2001). Lipids selected for the preparation of TSLs have relatively low melting phase transition temperatures. When this temperature is reached at mild hyperthermic conditions (39–42 °C), a liquid–crystalline phase transition occurs and increases the permeability and release of its contents (de Smet et al. 2011; Langereis et al. 2013). Pioneering reports suggesting the feasibility of such drug delivery systems for tumor treatment were published in the late 1970s by Yatvin et al. (1978), Weinstein et al. (1979). With modern-designed lipids and stealth liposomes, hyperthermia-induced drug release is now a realistic goal. A large number of studies have been published in the past decade investigating safer techniques and practices for use in patients. Hyperthermia can be induced by high intensity focused ultrasound (HIFU). MRI-guided HIFU is a non-invasive procedure already used in clinical practice (Tempany et al. 2003). It increases local temperatures deep inside targeted tissues by focusing US waves over a small, well-defined area (Deckers and Moonen 2010; Moonen 2007). The MRI-directed guidance enables in situ target definition and a highly localized treatment that spares healthy tissue (Tempany et al. 2003; Moonen 2007). Over the course of 15 years, Dewhirst and colleagues developed paramagnetic liposomes for the delivery of chemotherapeutic agents into tumors under mild hyperthermia (Ponce et al. 2007; Needham et al. 2000; Needham and Dewhirst 2001; Viglianti et al. 2004, 2006; Negussie et al. 2011). In an extensive longitudinal study, they elaborated the concept of "drug dose painting." This concept uses different protocols for hyperthermia with a real-time control of intratumoral drug distribution. Three hyperthermia protocols that used lysolipid-based temperature-sensitive liposomes (LTSLs) containing DOX and Mn as an MRI tracer (DOX/Mn-LTSLs) were evaluated in tumor-bearing rats (Fig. 7). In the first protocol, hyperthermia was initiated 15 min before the intravenous administration of DOX/Mn-LTSLs. For the second protocol, DOX/Mn-LTSLs were administered 15 min before hyperthermia. In the third protocol, half of the DOX/Mn-LTSL dose was administered before hyperthermia initiation and the other half was administered 15 min after a thermal steady state was reached. They found that rats administered with DOX/Mn-LTSLs during hyperthermia showed the best tumor response and demonstrated an MRI-monitored real-time drug dose "painting"

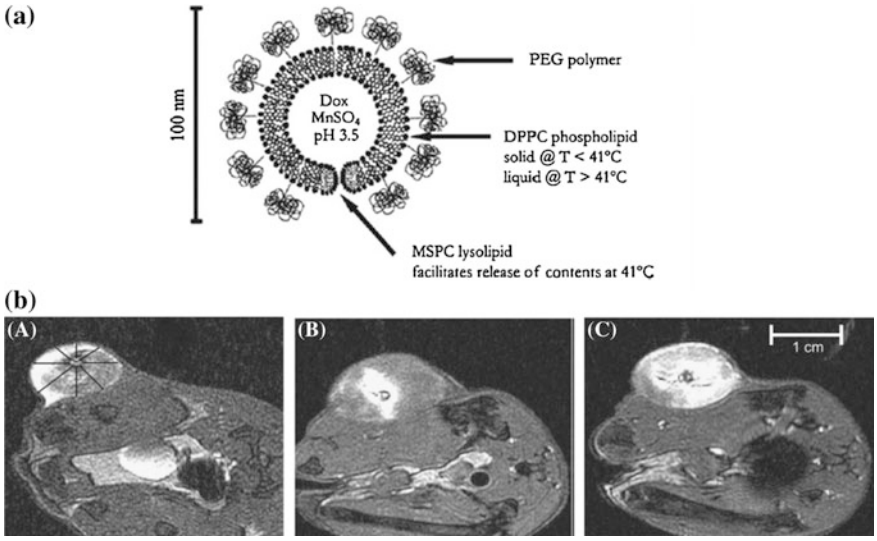

Fig. 7 **a** Schematic representation of a DOX/Mn-LTSL, theranostic temperature-sensitive liposome containing therapeutic DOX, and an MRI contrast agent, $MnSO_4$. **b** In vivo MRI images showing a tumor drug distribution after i.v. injection of DOX/Mn-LTSL to rats-bearing fibrosarcomas. *a* DOX/Mn-LTSL administered during steady-state hyperthermia. Radial lines depict the orientation of DOX concentration profile. *b* DOX/Mn-LTSL administered 15 min before the onset of hyperthermia resulted in central enhancement of DOX concentration. *c* Injection of DOX/Mn-LTSL both before and during hyperthermia show uniform drug distribution. Adapted from Ponce et al. (2007)

(Ponce et al. 2007). Unfortunately, the use of toxic Mn for MRI-mediated monitoring of the treatment response has thus far prevented the clinical development of DOX/Mn-LTSLs. In a proof-of-concept study in 9L glioblastoma-bearing rats, de Smet et al. developed temperature-sensitive liposomes (TSLs) encapsulated with DOX and [Gd(HPD03A)(H_2O)] complexes (de Smet et al. 2010). A HIFU-triggered release of imaging agents was monitored with interleaved T1 mapping of the tumor and correlated with DOX release. The results showed a good correlation between the averaged ΔR_1, changes across the tumor tissue, and the uptake of DOX. Because of high variations of inter-tumoral DOX concentrations, this study suggested that the uptake of therapeutic agents depended on the type of tumor and its pathophysiology (vascularization, permeability, and existence of a necrotic core) (de Smet et al. 2011). The feasibility of MR-HIFU using DOX-loaded LTSLs was recently shown to be efficient on a Vx2 rabbit tumor model (Ranjan et al. 2012).

During the development of MRI theranostics, the payload of contrast agents plays a critical role with respect to their toxicity. Agulla et al. compared the in vivo contrast for liposomal formulations containing different Gd concentrations. In their study, the intensity of the T1 effect was not linearly proportional with the liposomal Gd content. The liposomal formulation with the lowest concentration of Gd had the highest longitudinal relaxivity (Agulla et al. 2014b). This was in agreement with the

claim that the longitudinal relaxivity of paramagnetic liposomes was modulated in living cells by compartmentalization effects (Langereis et al. 2013).

4.2 Micelles

Micelles are self-assembling systems made of amphiphilic polymers with hydrophobic chains in the core and outward-facing hydrophilic moieties forming a corona. As is the case for liposomes, depending on the amphiphilicity of its constituents, micelles can have stealth properties and can be functionalized for active targeting (Torchilin 2004). Micelles used for drug delivery purposes have a diameter typically less than 100 nm (Straathof et al. 2011; Blanco et al. 2009; Torchilin 2007). Polymer micelles are stable, biocompatible systems that can solubilize a large palette of poorly water-soluble compounds (Blanco et al. 2009; Torchilin 2007; Matsumura et al. 2004). Different copolymers can be used for the preparation of micelles. Poly(propylene oxide) (PPO), PLA, poly(glycolide), PLGA, poly(ε-caprolactone) (PCL) (Blanco et al. 2009), poly(amino acid), and poly (trimethylene carbonate) (PTMC) are among the most widely used polymers in the hydrophobic core. The corona is mainly composed of hydrophilic polymers, such as PEG (Blanco et al. 2009; Torchilin 2007), poly(N-vinyl-2-pyrrolidone) (PVP) (Torchilin 2007), and PHPMAm (Talelli et al. 2010). Because micelles lack the aqueous core found in liposomes, both drug and an imaging agent can either be bound to the polymer, conjugated via an anchor molecule, or entrapped in its hydrophobic core (Janib et al. 2010; Torchilin 2007).

Kaida et al. prepared theranostic micelles incorporating gadolinium–diethylenetriaminepentaacetic acid (Gd–DTPA) and (1,2-diaminocyclohexane) platinum (II) (DACHPt; i.e., the parent complex of an anticancer agent oxaliplatin) into the hydrophobic moiety of poly(ethylene glycol)-block-poly(glutamic acid) [PEG-*b*-P (Glu)]. Compared with the free drug, these micelles showed a prolonged circulation time and strong anticancer effect in an orthotopic human pancreatic cancer model. Furthermore, an enhanced micelle-mediated MRI contrast of the tumor tissue was compared with that of the Gd–DTPA alone (Kaida et al. 2010).

Recently, polymer micelles incorporating radionuclides for SPECT and PET imaging have gained interest. Peng et al. reported on a multimodal system designed for the photothermal therapy of cancer that incorporated a NIR dye, IR-780, for fluorescence imaging, and ^{188}Re for SPECT imaging (Peng et al. 2011). The in vivo results of photothermal therapy induced by irradiation with a light dose of 540 J/cm^2 of NIR light showed an 82.6 % inhibition of tumor growth after 27 days. Treatment was successfully monitored with both NIR fluorescence imaging and micro SPECT/CT.

An entirely different approach for using micelles as theranostic vehicles was explored in the work of Wu et al. who described a first NIR dicyanomethylene-4*H*-pyran (DCM)-based prodrug, PEG–PLA/DCM-S-camptothecin (CPT), for the monitoring of the anticancer treatment in living animal models (Fig. 8). The

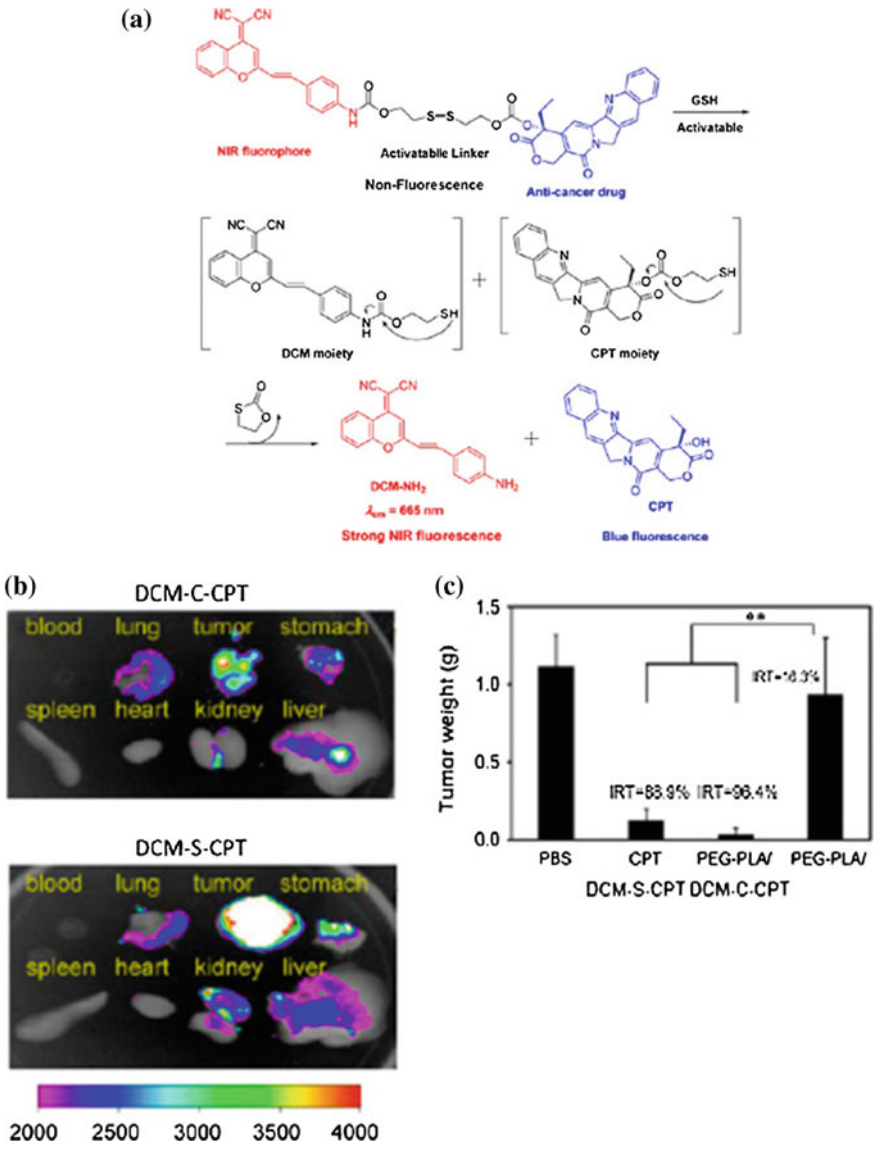

Fig. 8 **a** Scheme of proposed CPT release mechanism from the activated prodrug; **b** fluorescence intensity images of DCM-C-CPT and **c** DCM-S-CPT in internal organs after administration. Antitumor activities of PBS, CPT, and PEG–PLA micelles loaded with the C or S form of the prodrug administered at a dose of 5 mg/kg (CPT equivalents) to BCap-37 mice tumor model. As it can be seen from the histogram, PEG–PLA/DCM-S-CPT micelles inhibited tumor growth (IRT) when compared with the PEG–PLA/DCM-C-CPT and free CPT (*$p < 0.05$; **$p < 0.01$). Adapted from Wu et al. (2014)

prodrug itself was composed of the NIR fluorophore DCM and the anticancer drug CPT joined by a disulfide linker. The prodrug was loaded into PEG–PLA micelles to improve its water solubility and to achieve tumor targeting by the EPR effect (Wu et al. 2014). An advantage of the system was that both the fluorescence and cytotoxicity were initially quenched. When the micelles reached the tumor cells, the disulfide bonds were cleaved because of elevated intracellular glutathione levels. This enabled the drug release, which was monitored by the unquenched NIR fluorescence. The antitumor activity of these micelles was assessed in a BCap-37 tumor xenograft mouse model. Mice were intravenously administered with PBS, CPT, PEG–PLA/DCM-S-CPT, and PEG–PLA/DCM-C-CPT (with an alkane bond instead of a disulfide bond), at a CPT equivalent dose of 5 mg/kg. PEG–PLA/DCM-S-CPT showed a tumor inhibition rate of 96.4 % compared with 16.3 and 88.9 % for PEG–PLA/DCM-C-CPT and CPT alone, respectively. No severe systemic side effects were observed upon PEG–PLA/DCM-S-CPT treatment (Wu et al. 2014).

5 Inorganic Assemblies

In addition to organic polymers and lipids, various inorganic materials may be used in the preparation of NPs for drug delivery and imaging. These range from metals, such as iron, silver, or gold, and quantum dots (QDs), to carbon- and silica-based matrices. In the next section of this chapter, we will cover the area of iron oxide and gold NPs used in theranostics.

5.1 Iron Oxide NPs (IONPs)

Iron oxide NPs (IONPs) are made from hematite (Fe_2O_3) or magnetite (Fe_3O_4). These particles are paramagnetic, can serve as good T2 MRI contrast agents, and possess attractive physical properties for hyperthermic treatment. Superparamagnetic iron oxide NPs (SPIONs) are small IONPs (1–20 nm), mostly made from magnetite. The large specific surface area of IONP and SPIONs makes them suitable for the attachment of drugs and other ligands (Choi et al. 2012). Furthermore, their biodegradability, biocompatibility, and unique targeting possibilities controllable by an external magnetic field make them candidates for theranostic purposes (Santhosh and Ulrih 2013). Standard methods for the preparation of IONPs include co-precipitation (Xie et al. 2010; Santhosh and Ulrih 2013), microemulsification, thermal decomposition of iron precursors (Xie et al. 2010; Santhosh and Ulrih 2013), and hydrothermal methods (Santhosh and Ulrih 2013). New approaches for the production of monodispersed NPs use microwaves and sonochemical routes (Santhosh and Ulrih 2013). Silica (Algar et al. 2011),

phospholipids, or polymers, such as PEG, dextran, chitosan, PVP, and polyaniline, are typically added during their preparation (Xie et al. 2010; Santhosh and Ulrih 2013) to minimize oxidation, avoid NP aggregation, and tailor their surfaces for further attachment of functional groups and drugs (Xie et al. 2010).

Considering IONPs, we first examine the results of passive targeting nanosystems. Then, different active targeting strategies will be discussed. Quan et al. (2011) developed human serum albumin (HSA)-coated IONPs loaded with DOX (DOX-HSA-IONPs). NPs were prepared by adding DOX and dopamine-coated IONPs into an HSA-containing aqueous solution. Because HSA has a good ligand-binding capacity, a high loading rate was achieved for both DOX and IONPs [the DOX/Fe/HSA ratio was 1:2:20 (w/w/w)]. The efficacies of the DOX-HSA-IONPs, commercial Doxil® liposomes, and free DOX were evaluated on a 4T1 murine breast cancer model. Particle uptake upon administration was monitored by MRI. MR images taken 1 and 4 h after the injection of DOX-HSA-IONPs showed a signal decrease as a result of NP accumulation in the tumor area. The efficacy of DOX-HSA-IONPs in tumor suppression was comparable with that of Doxil® and outperformed free DOX treatment (Quan et al. 2011).

Another passive targeting nanotheranostic system was developed by Yu et al. who incorporated DOX into the polymer shell of thermally cross-linked (TCL) SPIONs (TCL-SPIONs) through electrostatic interactions with polymer coating layers. For the validation of the therapeutic efficacy of DOX-TCL-SPIONs, mice-bearing Lewis lung carcinoma was used. It was demonstrated that DOX-TCL-SPIONs primarily localized in tumors. Because of their SPION content, these nanosystems were precisely localized by MRI. In this case, the DOX-TCL-SPIONs gave a superior therapeutic outcome when compared with free DOX. No systemic toxicity was reported (Yu et al. 2008).

As mentioned above, the surface of iron oxide particles can be functionalized with specific moieties targeting overexpressed proteins. IONPs targeting the receptor of uPA (uPAR) were conjugated with the amino-terminal fragment (ATF) peptide of the receptor-binding domain of uPA and the chemotherapeutic drug gemcitabine (GEM) via the cathepsin B cleavable peptide linker (GFLG). In vivo experiments were carried out in the orthotopic tumor xenografts with MIA PaCa-2 human pancreatic cancer cells in nude mice. Mice were divided into groups administered with free GEM, ATF-IONP-GEM, and IONP-GEM (without any targeting moieties). A 2 mg/kg GEM-equivalent dose was given to mice twice a week for five times. T2 MR images were acquired before the treatment and 1 and 2 weeks following the treatment (Fig. 9). Mice treated with ATF-IONP-GEM showed an approximate 50 % inhibition of tumor growth in comparison with 30 and 23 % by free GEM and nontargeted IONP-GEM, respectively. Moreover, the conjugation of GEM to the NPs improved the stability of the drug in vivo by preventing its deactivation by cytidine deaminase (Lee et al. 2013). This study is one of many that showed the effectiveness of active targeting. Additionally, it showed the potential of using IONPs to monitor the accumulation of nanosystems in targeted tissues and confirmed a sustained drug release.

"Magnetic drug targeting" is a term introduced by Alexiou et al. (2000). In their experiments, mitoxantrone (MTX), an antineoplastic agent, was bound to

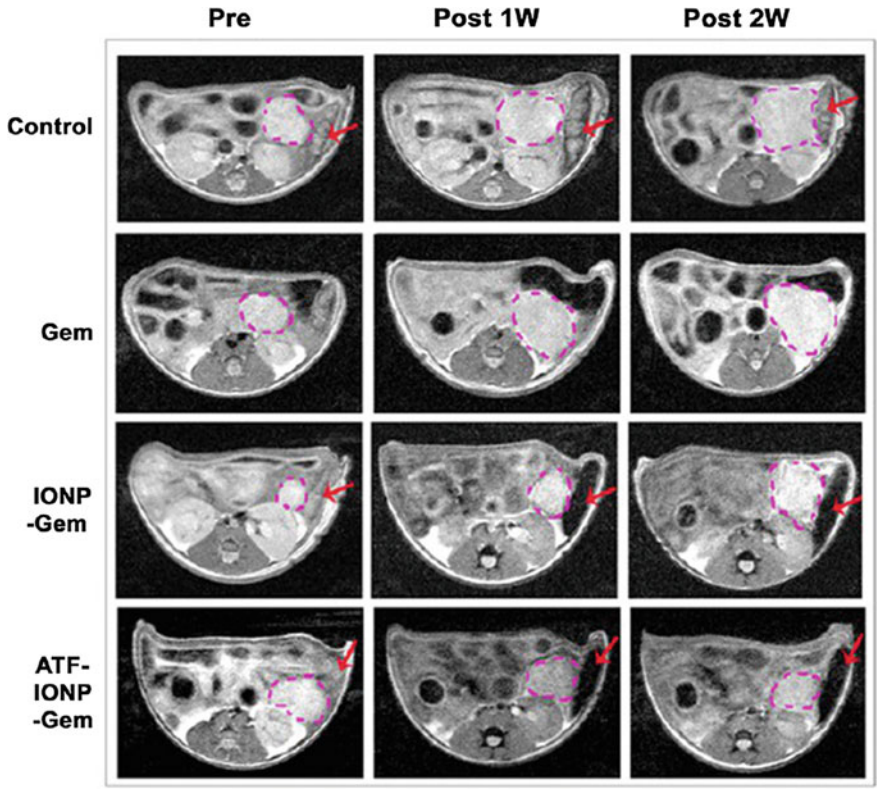

Fig. 9 Axial T2-weighted MRI images of tumor-bearing mice before, 1 (1 W) and 2 weeks (2 W) upon NPs administration. Post 1W and post 2W images were obtained 48 h after second and third injections, respectively. *Pink-dotted circles* mark tumor location and size, whereas *red arrows* show the MRI contrast change in the spleen. Adapted from Lee et al. (2013)

multi-domain NPs formed from iron oxides and hydroxides (ferrofluids), which were then coated with starch polymers. The colloidal dispersions of the ferrofluid-MTX were administered to female New Zealand White rabbits inoculated with VX-2 squamous cell carcinoma. An inhomogeneous magnetic field produced by an electromagnet was used to direct the ferrofluid-MTX to the tumor. High concentrations of the construct in the tumor tissue were confirmed by MRI and histology. This magnetic drug targeting approach led to the complete remission of the tumors with reduced doses of 20 and 50 % by the ferrofluid-MTX relative to the conventional MTX dose. The therapy was well-tolerated and showed no signs of toxicity (Alexiou et al. 2000). Although promising in animal studies, this approach seems difficult to be translated to humans.

5.2 Gold NPs (AuNPs)

Gold NPs (AuNPs) range in size between 1 and 100 nm. Depending on their size and shape, their optical properties are characterized by strong absorption and light scattering in the vis–NIR region (Algar et al. 2011; Alkilany et al. 2012; Boisselier and Astruc 2009; Chen et al. 2010; Khlebtsov et al. 2013; Zhang et al. 2013). Another important feature of AuNPs is the phenomenon of localized surface plasmon resonance (LSPR) (Khlebtsov 2008). Upon light irradiation at the proper frequency, the electrons in the conduction band of gold atoms are excited and begin to oscillate, which leads to extensive light extinction. For gold nanospheres, a broad LSPR band is observed at approximately 520 nm. In gold nanorods (AuNRs), the LSPR band splits into a transverse band and a longitudinal band. Their positions are dependent on the length and width of AuNRs. Additionally, AuNRs can be used for the photothermal therapy. AuNPs have been tested for the photodynamic treatment of pathogenic bacteria and photothermal cancer therapy (Khlebtsov et al. 2013). Furthermore, AuNPs have been used to quench the fluorescence of different fluorophores (Algar et al. 2011) and are capable of increasing the fluorescence quantum yield of NIR dyes up to 80 % (Bardhan et al. 2009). Gold is considered an inert metal, but there are a number of synthetic methods to tune the size and shape of AuNP and to chemically bind various molecules to their surface, such as MRI, fluorescence reporters, and therapeutic moieties, for multimodal theranostic applications (Alkilany et al. 2012). These characteristics make AuNPs suitable contrast agents for in vivo fluorescence imaging and valuable theranostic entities.

One of the most advanced nanosystems in use in photothermal tumor ablation by NIR-absorbing AuNPs is AuroLase™. This system is a PEGylated gold nanoshell formulation prepared by the absorption of colloidal gold to amine groups on silica NPs (O'Neal et al. 2004). Results observed after i.v. administration to both rodents (O'Neal et al. 2004) and dogs (Schwartz et al. 2009) showed the accumulation of nanoshells in tumor tissue via the EPR effect. Irradiation with light at 80 nm led to heat dissipation by the AuNPs and consequently, tumor eradication by thermal ablation, as indicated by MRI based on the temperature-dependent proton resonance frequency shift (Schwartz et al. 2009).

The search for multimodal imaging techniques to further improve diagnosis and monitoring is intensifying. One way to overcome the limitations of single imaging modalities is to design platforms to carry several complementary imaging probes (Louie 2010). One example is a platform using gold nanoshells covered with a layer of silica entrapping Fe_3O_4 NPs and the NIR fluorophore indocyanine green (ICG). These particles were intended to have dual diagnostic features and photothermal ablative properties. Because silica enables the attachment of various moieties, additional anti-HER2 antibodies were conjugated to the particles (Bardhan et al. 2009). Furthermore, PEG was added to decrease their immunogenic potential and to increase their blood circulation time (Bardhan et al. 2010). Tests were performed in mice inoculated with either BT474AZ cells highly overexpressing HER2 or MDAMB231 cells with low HER2 expression. NIR images were obtained at 0.3, 2, 4, 24, 48, and

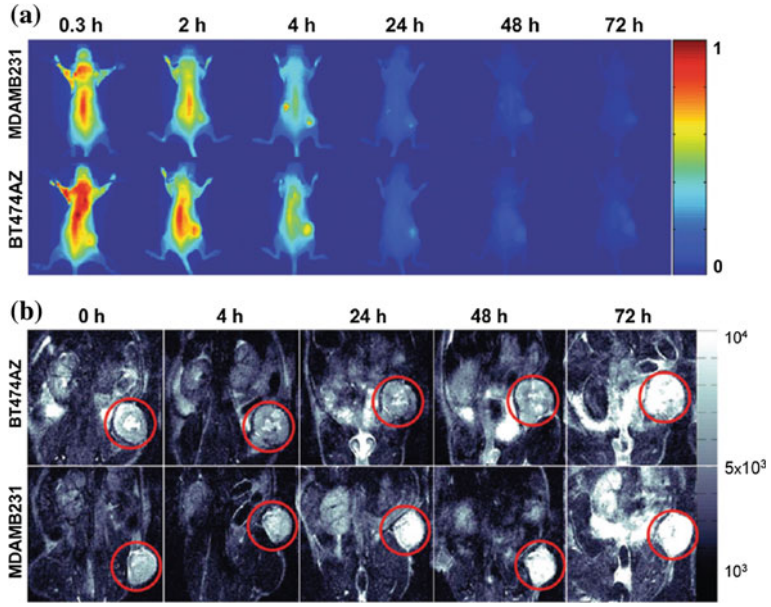

Fig. 10 Imaging of nanocomplex delivery. **a** NIR fluorescence images of mice with HER2 overexpressing BT474AZ xenografts and MDAMB231 (control) xenografts. Images were taken at 0.3, 2, 4, 24, 48, and 72 h post-injection. **b** T2-weighted images of BT474AZ and MDAMB231 mice before and 0, 4, 24, 48, and 72 h after administration. Tumors are marked with *red circles*. Adapted from Bardhan et al. (2010)

72 h post-injection with highest fluorescence intensity observed at 4 h. The results showed significant variations between the two xenograft models indicating the efficacy of the antibody-mediated active targeting strategy. This result was confirmed by T2 MRI (Fig. 10). However, a certain difference in NP accumulation across time points can be seen when the fluorescence images were compared with the MRI. The authors explained these discrepancies by the intrinsic differences between the NIR and MR imaging. In short, this study provided an example of a theranostic agent for thermoablation with simultaneous NIR and MR imaging features for the active targeting of HER2-positive breast carcinoma (Bardhan et al. 2010).

As mentioned above, active targeting is often achieved by attaching antibodies to NPs. A probe made from AuNR covalently linked to a low-molecular weight chitosan (M_w 5000), capped with 11-mercaptoundecanoic acid (MUA) and conjugated to the epithelial growth factor receptor (EGFR) monoclonal antibody, was described by Charan et al. (2012). In vitro and in vivo studies showed the selectivity of this theranostic probe for the specific targeting of cancer cells overexpressing EGFR. Furthermore, no significant toxicity was observed in mice injected with the AuNR nanocomplexes.

Gold particles can also be used for PDT. PEGylated AuNRs loaded with a phthalocyanine capable of dual photothermal and PDT were tested in xenograft mice (Jang et al. 2011). Treatment was monitored by NIR imaging. For mice

injected with AuNR and irradiated with NIR light, terminal deoxynucleotidyl transferase dUTP nick end labeling technique (TUNEL) showed a high degree of tissue damage and apoptosis across the tumor area compared with mice treated with PBS (control) or PDT only.

Another complex theranostic nanoconstruct was recently created by Topete et al. (2014). It was composed of a PLGA matrix loaded with DOX and covered with a porous shell of gold. To provide the nanoparticle with stealth properties, the surface was functionalized with HSA. ICG was attached for both imaging and PDT purposes. Active targeting was provided by the covalent conjugation of folic acid. Preliminary in vivo results were obtained on BALB/c nude mice inoculated with folic acid receptor-overexpressing MDA-MB-231 breast cancer cells. NIR fluorescence was monitored intravitally during treatment. An accumulation of these theranostic nanoconstructs was observed in tumor tissue and in the brain, which was surprising and would deserve confirmation (Topete et al. 2014).

6 Quantum Dots (QDs)

Quantum dots (QDs) are nanocrystals (2–10 nm) made from semiconducting materials. For biomedical applications, the QD cores are usually made from CdSe or CdTe and coated with ZnS for improvement of luminescent properties (Algar et al. 2011). Compared with standard organic fluorophores, QDs have up to 100 times improved brightness, photostability, and resistance to photobleaching. Additionally, QDs have wide excitation bands and narrow emission windows (Janib et al. 2010). QDs are now extensively investigated for their incorporation in imaging nanoconstructs. However, synthetic routes for QDs have resulted in insoluble and hydrophobic materials. Therefore, bifunctional ligand coating and bifunctional covalent attachment have been employed to overcome these limitations (Algar et al. 2011). Furthermore, efforts have been made to increase the stability, biocompatibility, and blood circulation of QDs. NIR QD-loaded PEG-10,12-pentacosydonic acid micelles equipped with trastuzumab conjugates for active targeting showed 77.3 % tumor growth inhibition when injected into athymic BALB/c-nu/nu nude mice-bearing HER2 positive tumors. NIR images showed a rapid distribution of micelles and their accumulation at the tumor sites (Nurunnabi et al. 2010). Although, these theranostic micelles did not show signs of toxicity, more experiments are required to assure the safety and complete clearance of QDs from the body.

7 Theranostic Application of Antibodies

Trastuzumab (Herceptin®), rituximab (Rituxan®), bevacizumab (Avastin®), cetuximab (Erbitux®), and panitumumab (Vectibix®) are among many examples of Food and Drug Administration in the United States of America (FDA) approved

therapeutic antibodies for cancer treatment (Accardo et al. 2013; Fleuren et al. 2014). Antibodies can be modified with radioactive tracers and fluorescent dyes for use in disease diagnosis and monitoring. This approach facilitates the selection of patients who are likely to respond to targeted antibody treatments. A comprehensive review on the theranostic applications of antibodies in oncology was recently published by Fleuren et al. (2014). Here, we will address only a few examples of these theranostic agents. ^{177}Lu-J591 is a humanized radiolabeled monoclonal antibody against prostate-specific membrane antigen (Bander et al. 2005). ^{177}Lu-J591 emits both β and γ-rays, which make this antibody conjugate well-suited for theranostic purposes. β-rays will enable the disease treatment, while γ-rays will serve as imaging tracers. In a phase II clinical trial, the response rate in patients was assessed. ^{177}Lu-J591 administration was well-tolerated and exhibited accurate tumor targeting capabilities. Additionally, prostate-specific antigen responses were in accordance with dose response (Tagawa et al. 2013). Another example of a potentially successful theranostic agent for treatment prediction is a chimeric antibody ^{177}Lu-girentuximab (^{177}Lu-cG250), which was developed for the treatment of metastatic clear cell renal cell carcinoma. This antibody binds to a heat-sensitive transmembrane glycoprotein carbonic anhydrase IX (CAIX). A phase I clinical study showed that ^{177}Lu-cG250 was well-tolerated in patients, could be repetitively administered, and could prevent the progression of the disease (Stillebroer et al. 2013). Apart from their application as theranostic agents, the use of antibodies, especially those having fluorescent tags, is also potentially applicable for imaging-assisted surgery (Heath et al. 2012; Muselaers et al. 2014). However, this is beyond the scope of this chapter.

8 Nanotheranostic Systems for Gene Therapy

Gene therapy was initially intended to be used to treat hereditary diseases; however, it also has high potential in cancer treatment (Devi 2006). Vectors for gene delivery are viral or non-viral. Although good results of gene transfer were obtained with viral vectors, their use still raises important issues about their safety because a few vectors may induce mutagenesis and can cause unwanted immune responses in patients. Functionalized gold NPs, carbon nanotubes, polymer NPs, and cationic polymers are examples of non-viral gene vectors (Wang et al. 2012; Mok and Park 2012). Among them, polymer particles have shown potential in delivering nucleic acids to cells and are now being investigated for theranostic purposes. One example of these complex structures is a core–shell NP produced by the SPION loading of mPEG–PLA micelles for the delivery of plasmid DNA coated with cationic polymers (chitosan and PEI). These NPs are designed for T2-weighed MRI and gene delivery and have shown efficient cell transfection in vitro and in vivo (Wang et al. 2012). Multifunctional chitosan magnetic-graphene NPs are also promising theranostic gene/drug delivery vehicles (developed by the same group). These SPION-loaded NPs simultaneously deliver plasmid DNA and DOX to implanted

tumors in mice and were suitable for MRI (Wang et al. 2013). The gene Survivin, an inhibitor of apoptosis, is upregulated in many types of cancer. Because this gene is not expressed in normal cells, it presents a valuable target for gene silencing by siRNA. Theranostic liposomes were prepared from the combination of following compounds: Gd-DOTA-DSA, CDAN, DOPC, DSPE-PEG^{2000}, and DOPE rhodamine through the rehydration and sonication of lipid films. Anti-Survivin siRNA was then added by intensive vortex mixing. Liposomes were intravenously administered into mice carrying OVCAR-3, human ovarian cancer cells. T1 MR images showed increased signal intensity upon treatment. Tumor growth was reduced in comparison with the non-silencing negative controls. Fluorescence microscopy imaging confirmed the colocalization of liposomes and siRNA in the tumor (Kenny et al. 2011). These multifunctional nanocarriers are promising systems for the future of gene delivery approaches for the treatment of cancers.

9 Discussion

Early diagnosis is of utmost importance in providing efficient treatment to patients suffering from diseases such as cancer. With respect to cancer detection, the most encountered problems with most imaging modalities are low detection limits. In general, tumor masses must contain at least 10^9 cells (having a volume of approximately 1 cm^3) (Frangioni 2008) to be detectable by conventional imaging techniques. The difficulty in developing a successful theranostic agent is in optimizing the concentration of the imaging probe to provide a sufficient SBR and a sufficient concentration of active pharmaceutical ingredient in a single vehicle. The recent development of nanotechnology provides the opportunity to confine multiple imaging modalities within the same carrier. Today, we are able to visualize pathophysiological processes, such as changes in enzyme regulation or DNA and RNA expressions at cellular and molecular levels. This so-called molecular imaging will be important for the early diagnoses of diseases where phenotypic changes in cells are not yet evident (Weissleder 1999, 2002; Mulder et al. 2007). Theranostic agents have the ability to monitor and control the location, dose, and time of drug delivery and provide a real-time feedback of a given treatment. This enables the adjustment of subsequent treatments for an individualized therapeutic approach. Multimodal theranostic NPs enable molecular imaging because of the complementary functions of two or more imaging agents colocalizing at the target site (Louie 2010; Thorsen et al. 2013). Examples of these multi-imaging constructs are particles capable of simultaneous MRI and fluorescence imaging. MRI provides excellent anatomical visualizations at high resolutions, but is limited by nonspecific interactions and requires large quantities of imaging agent. Optical fluorescence is very sensitive, has a high SBR, and can detect molecular changes at the cellular level (Mulder et al. 2007). Multimodal delivery systems provide advantages in single administration and have the same pharmacokinetic profile for each modality found in NPs. However, the development of this type of nanosystems requires careful planning of synthesis procedures in order to

attach two entities with different chemical properties or imaging probes whose sensitivities may vary among each other up to three orders of magnitude (Louie 2010).

The encapsulation of small molecules into nanocarriers or their conjugation with polymers changes their properties. It increases the solubility of hydrophobic molecules by orders of magnitude; alters the pharmacokinetic profile, biodistribution, and clearance properties; and reduces systemic toxicity. Nevertheless, there are a number of requirements that need to be fulfilled for a clinically applicable nanotheranostic system. In this sense, polymer NPs present a valuable option for the future development of theranostic agents as long as the polymers used in their preparation fulfill the following criteria: the manufacturing process should be easily scaled up, linkages on the NP surface should be stable, and the specific activities of the attached moieties should not be affected during the NP preparation. Moreover, coupling chemistry protocols should be compatible with future medical applications (Algar et al. 2011). Additionally, nanosystems need to be sterile. Up to date, it is still difficult to have sterilization protocols that do not alter the physico-chemical properties of the nanotheranostic formulations. Another challenge in the development and the approval of polymer nanosystems is the natural heterogenicity of polymers. This, along with the need to incorporate a large number of entities to NP surface for the theranostic application, ultimately leads to complex characterization methods (Duncan 2003; Yuan et al. 1995).

As mentioned earlier, the chances of better therapeutic outcome lie in the active targeting of diseased tissues. Successful active targeting is very difficult to achieve due to the limited number of highly specific cell surface epitopes expressed at the appropriate locations. One of the key factors for the development of an efficient therapy is regulating the particle sizes of the constructs to control their ability to cross barriers, including basement membranes, endothelial cell linings, and in some cases the blood–brain barrier. It has been shown that the accumulation of drug delivery systems in solid tumors depends on the tumor type and on the fenestration of tumor blood vessels (Yuan et al. 1995). Recent progress in the field of molecular biology and organic synthesis has made it possible to identify and couple small ligands with specific targeting capabilities onto the surface of NPs. The attachment of small molecules generally favors penetration into tissues, induces fewer immunogenic reactions, and provides better pharmacological and pharmacokinetic properties (Weissleder 2001). In addition to size, other physical characteristics of administered NPs, such as the polymer used in their synthesis, PEGylation, and attached ligands, all play important role in the ability of formulations to reach and accumulate at the tumor site (Iyer et al. 2006). Nevertheless, the EPR effect has mainly been proven in small animals and rarely shown in humans. Murine tumors are induced by a subcutaneous or orthotopical injection of previously cultured cancer cells which are not submitted to immune pressure. These fast-growing tumors lack genetic diversity and they form blood vessels unlike those in the human body. In this case much care is required when extrapolating results from preclinical in vivo pharmacokinetics and biodistribution studies to humans (Nichols and Bae 2014).

There are many questions concerning the safety of nanomedicines. This particularly applies to metals and polymers used in the composition of nanoconstructs.

During initial phases of the NP development, cellular assays such as the 3-[4,5-dimethylthiazol-2-yl]-2,5-diphenyl tetrazolium bromide (MTT) or lactate dehydrogenase (LDH) assays are usually employed to determine the toxic potential of their components (Haglund et al. 2009). However, these types of assays do not reflect the real situation. Hence, acute and chronic toxicity tests should be conducted in all cases.

10 Conclusion and Future Perspectives

The field of nanomedicine is growing rapidly giving rise to fascinating new platforms and constructs that might provide new solutions for the expansion of theranostics. Recent avenues in nanomaterials are in the field of photopolymerizable lipids (Puri and Blumenthal 2011). Liposomes made from this type of lipid can be used for light-triggered drug release as shown by Yavlovich et al. (2011). Moreover, a new imaging modality is emerging for the early detection of cancer based on Raman spectroscopy (Nijssen et al. 2009). Nanoparticle-based combination chemotherapy with particles loaded with two drug–polymer conjugates have also been recently reported (Aryal et al. 2011). This controlled dual drug loading may serve in creating improved polymer platforms for theranostics.

It has been shown that the enhanced nanoparticle retention at tumor sites is achieved when an active targeting approach is used. Hence, the future of theranostic nanomedicine lies in a hetero-multivalent ligand design of NPs. This would enable co-operative binding interactions for further improving targeting capabilities (Modery-Pawlowski and Gupta 2014). Another solution for the efficient active targeting of multimodal NPs could be found in a protease-removable polymer coating that veils attached ligands. Once the hydrophilic polymer is cleaved, the attached moieties become exposed and can be activated (Harris et al. 2008).

Additionally, Förster resonance energy transfer (FRET)-activated self-immolative linker designs (Redy and Shabat 2012) show promise for prodrug activation monitoring in vivo and can provide information about the specific location and concentration of activated drugs in tissues.

Dendrimers, a class of well-defined multifunctional polymer nanoconstructs, may also be a good solution for the development of theranostics. Dendrimers are hyperbranched polymer macromolecules suitable for the controlled orthogonal attachment of different moieties for drug transport, imaging, and targeting (Ornelas et al. 2011; Cai et al. 2013). Many patients have already been filed and then papers published on dendrimer synthesis and their use in theranostics for photothermal therapy (Li et al. 2014), PDT (Sibani et al. 2008; Taratula et al. 2013; Klajnert et al. 2012), and conventional drug targeting (Huang et al. 2014). In spite of their high potential, dendrimer synthesis is a relatively expensive multistep process that may present problems for scale-up productions.

As mentioned, microbubbles are another possible platform for drug delivery (Eisenbrey et al. 2009, 2010a, b; Cochran et al. 2011). As one of the major causes

of death in the world, stroke has limited timeframe for treatment application. Currently, the recombinant tissue plasminogen activator (rtPa) is the only thrombolytic drug approved by the FDA and European Medicines Agency (EMA) for the treatment of ischemic stroke (Petit et al. 2012a). Petit et al. (2012b) observed a synergistic effect of US, microbubbles, and rtPa on clot lysis. Although it is not exactly the type of theranostics described in this chapter, microbubbles loaded with rtPa and equipped with a targeting ligand could potentially provide better treatment outcomes than the aforementioned theranostic procedures. Additionally, microbubbles are interesting for multimodal imaging purposes. Recently, Huynh et al. (2014) reported a microbubble formulation prepared by the substitution of 50 % molar regular phospholipid (DSPC) with a porphyrin–lipid. These microbubbles were injected into mice-bearing KB tumor xenografts and imaged by US, PAI, and fluorescence. Although the microbubbles burst upon US application, the porphyrin–lipid composition enabled the real-time tracking using PAI and fluorescence imaging. Microbubbles with the abovementioned properties are promising theranostic agents.

Although theranostics shows great potential for the development of medicine, there have only been a few theranostic agents that have reached clinical trials. The most advanced ones seem to be thermosensitive liposomes for HIFU treatment, AuNPs for tumor thermoablation, and Ab conjugates used in radioimmunotherapy.

Acknowledgments NL's work is supported by the Grants Nos. 205320_138309, CR32I3_129987, CR32I3_147018, 31003A_149962, and CR32I3_150271 of the Swiss Science Foundation.

References

Accardo A, Tesauro D, Morelli G (2013) Peptide-based targeting strategies for simultaneous imaging and therapy with nanovectors. Polym J 45(5):481–493

Adams KE, Ke S, Kwon S, Liang F, Fan Z, Lu Y et al (2007) Comparison of visible and near-infrared wavelength-excitable fluorescent dyes for molecular imaging of cancer. J Biomed Opt 12(2):024017

Agulla J, Brea D, Campos F, Sobrino T, Argibay B, Al-Soufi W et al (2014a) In vivo theranostics at the peri-infarct region in cerebral ischemia. Theranostics 4(1):90–105

Agulla J, Brea D, Argibay B, Novo M, Campos F, Sobrino T et al (2014b) Quick adjustment of imaging tracer payload, for in vivo applications of theranostic nanostructures in the brain. Nanomed Nanotechnol Biol Med 10(4):851–858

Alexiou C, Arnold W, Klein RJ, Parak FG, Hulin P, Bergemann C et al (2000) Locoregional cancer treatment with magnetic drug targeting. Cancer Res 60(23):6641–6648

Algar WR, Prasuhn DE, Stewart MH, Jennings TL, Blanco-Canosa JB, Dawson PE et al (2011) The controlled display of biomolecules on nanoparticles: a challenge suited to bioorthogonal chemistry. Bioconjug Chem 22(5):825–858

Alkilany AM, Thompson LB, Boulos SP, Sisco PN, Murphy CJ (2012) Gold nanorods: their potential for photothermal therapeutics and drug delivery, tempered by the complexity of their biological interactions. Adv Drug Deliv Rev 64(2):190–199

Aryal S, Hu CM, Zhang L (2011) Polymeric nanoparticles with precise ratiometric control over drug loading for combination therapy. Mol Pharm 8(4):1401–1407

Bander NH, Milowsky MI, Nanus DM, Kostakoglu L, Vallabhajosula S, Goldsmith SJ (2005) Phase I trial of 177lutetium-labeled J591, a monoclonal antibody to prostate-specific membrane antigen, in patients with androgen-independent prostate cancer. J Clin Oncol 23(21):4591–4601

Bardhan R, Chen WX, Perez-Torres C, Bartels M, Huschka RM, Zhao LL et al (2009) Nanoshells with targeted simultaneous enhancement of magnetic and optical imaging and photothermal therapeutic response. Adv Funct Mater 19(24):3901–3909

Bardhan R, Chen WX, Bartels M, Perez-Torres C, Botero MF, McAninch RW et al (2010) Tracking of multimodal therapeutic nanocomplexes targeting breast cancer in vivo. Nano Lett 10(12):4920–4928

Beer AJ, Schwaiger M (2008) Imaging of integrin alpha v beta 3 expression. Cancer Metastasis Rev 27(4):631–644

Blanco E, Kessinger CW, Sumer BD, Gao J (2009) Multifunctional micellar nanomedicine for cancer therapy. Exp Biol Med 234(2):123–131

Boisselier E, Astruc D (2009) Gold nanoparticles in nanomedicine: preparations, imaging, diagnostics, therapies and toxicity. Chem Soc Rev 38(6):1759–1782

Bussolati B, Grange C, Bruno S, Buttiglieri S, Deregibus MC, Tei L et al (2006) Neural-cell adhesion molecule (NCAM) expression by immature and tumor-derived endothelial cells favors cell organization into capillary-like structures. Exp Cell Res 312(6):913–924

Cai XP, Hu JJ, Xiao JR, Cheng YY (2013) Dendrimer and cancer: a patent review (2006–present). Expert Opin Ther Pat 23(4):515–529

Caravan P (2006) Strategies for increasing the sensitivity of gadolinium based MRI contrast agents. Chem Soc Rev 35(6):512–523

Charan S, Sanjiv K, Singh N, Chien FC, Chen YF, Nergui NN et al (2012) Development of chitosan oligosaccharide-modified gold nanorods for in vivo targeted delivery and noninvasive imaging by NIR irradiation. Bioconjug Chem 23(11):2173–2182

Chen XY, Hou YP, Tohme M, Park R, Khankaldyyan V, Gonzales-Gomez I et al (2004) Pegylated Arg-Gly-Asp peptide: Cu-64 labeling and PET imaging of brain tumor alpha(v)beta(3)-integrin expression. J Nucl Med 45(10):1776–1783

Chen JY, Yang MX, Zhang QA, Cho EC, Cobley CM, Kim C et al (2010) Gold nanocages: a novel class of multifunctional nanomaterials for theranostic applications. Adv Funct Mater 20 (21):3684–3694

Chen X, Gambhir SS, Cheon J (2011) Theranostic nanomedicine. Acc Chem Res 44(10):841

Cheng L, Yang K, Chen Q, Liu Z (2012) Organic stealth nanoparticles for highly effective in vivo near-infrared photothermal of cancer. ACS Nano 6(6):5605–5613

Choe R, Konecky SD, Corlu A, Lee K, Durduran T, Busch DR et al (2009) Differentiation of benign and malignant breast tumors by in-vivo three-dimensional parallel-plate diffuse optical tomography. J Biomed Opt 14(2):024020

Choi KY, Liu G, Lee S, Chen X (2012) Theranostic nanoplatforms for simultaneous cancer imaging and therapy: current approaches and future perspectives. Nanoscale 4(2):330–342

Cochran MC, Eisenbrey J, Ouma RO, Soulen M, Wheatley MA (2011) Doxorubicin and paclitaxel loaded microbubbles for ultrasound triggered drug delivery. Int J Pharm 414(1–2):161–170

Danhier F, Ansorena E, Silva JM, Coco R, Le Breton A, Preat V (2012) PLGA-based nanoparticles: an overview of biomedical applications. J Control Release 161(2):505–522

Davies GL, Kramberger I, Davis JJ (2013) Environmentally responsive MRI contrast agents. Chem Commun 49(84):9704–9721

de Smet M, Langereis S, van den Bosch S, Grull H (2010) Temperature-sensitive liposomes for doxorubicin delivery under MRI guidance. J Control Release 143(1):120–127

de Smet M, Heijman E, Langereis S, Hijnen NM, Grull H (2011) Magnetic resonance imaging of high intensity focused ultrasound mediated drug delivery from temperature-sensitive liposomes: an in vivo proof-of-concept study. J Control Release 150(1):102–110

Deckers R, Moonen CTW (2010) Ultrasound triggered, image guided, local drug delivery. J Control Release 148(1):25–33

Delli Castelli D, Dastru W, Terreno E, Cittadino E, Mainini F, Torres E et al (2010) In vivo MRI multicontrast kinetic analysis of the uptake and intracellular trafficking of paramagnetically labeled liposomes. J Control Release 144(3):271–279

Devi GR (2006) siRNA-based approaches in cancer therapy. Cancer Gene Ther 13(9):819–829

Dijkmans PA, Juffermans LJ, Musters RJ, van Wamel A, ten Cate FJ, van Gilst W et al (2004) Microbubbles and ultrasound: from diagnosis to therapy. Eur J Echocardiogr 5(4):245–256

Duncan R (2003) The dawning era of polymer therapeutics. Nat Rev Drug Discov 2(5):347–360

Eisenbrey JR, Huang P, Hsu J, Wheatley MA (2009) Ultrasound triggered cell death in vitro with doxorubicin loaded poly lactic-acid contrast agents. Ultrasonics 49(8):628–633

Eisenbrey JR, Soulen MC, Wheatley MA (2010a) Delivery of encapsulated Doxorubicin by ultrasound-mediated size reduction of drug-loaded polymer contrast agents. IEEE Trans Bio Med Eng 57(1):24–28

Eisenbrey JR, Burstein OM, Kambhampati R, Forsberg F, Liu JB, Wheatley MA (2010b) Development and optimization of a doxorubicin loaded poly(lactic acid) contrast agent for ultrasound directed drug delivery. J Control Release 143(1):38–44

Fleuren EDG, Versleijen-Jonkers YMH, Heskamp S, van Herpena CML, Oyen WJG, van der Graaf WTA, Boerman OC (2014) Theranostic applications of antibodies in oncology. Mol Oncol 8:799–812

Frangioni JV (2008) New technologies for human cancer imaging. J Clin Oncol 26(24):4012–4021

Furgeson DY, Dreher MR, Chilkoti A (2006) Structural optimization of a "smart" doxorubicin-polypeptide conjugate for thermally targeted delivery to solid tumors. J Control Release 110(2):362–369

Gabriel D, Busso N, So A, van den Bergh H, Gurny R, Lange N (2009) Thrombin-sensitive photodynamic agents: a novel strategy for selective synovectomy in rheumatoid arthritis. J Control Release 138(3):225–234

Gabriel D, Zuluaga MF, van den Bergh H, Gurny R, Lange N (2011) It is all about proteases: from drug delivery to in vivo imaging and photomedicine. Curr Med Chem 18(12):1785–1805

Ganta S, Devalapally H, Shahiwala A, Amiji M (2008) A review of stimuli-responsive nanocarriers for drug and gene delivery. J Control Release 126(3):187–204

Gao FP, Lin YX, Li LL, Liu Y, Mayerhoffer U, Spenst P et al (2014) Supramolecular adducts of squaraine and protein for noninvasive tumor imaging and photothermal therapy in vivo. Biomaterials 35(3):1004–1014

Geninatti Crich S, Bussolati B, Tei L, Grange C, Esposito G, Lanzardo S et al (2006) Magnetic resonance visualization of tumor angiogenesis by targeting neural cell adhesion molecules with the highly sensitive gadolinium-loaded apoferritin probe. Cancer Res 66(18):9196–9201

Grange C, Geninatti-Crich S, Esposito G, Alberti D, Tei L, Bussolati B et al (2010) Combined delivery and magnetic resonance imaging of neural cell adhesion molecule-targeted doxorubicin-containing liposomes in experimentally induced Kaposi's sarcoma. Cancer Res 70(6):2180–2190

Hagendoorn J, Tong R, Fukumura D, Lin Q, Lobo J, Padera TP et al (2006) Onset of abnormal blood and lymphatic vessel function and interstitial hypertension in early stages of carcinogenesis. Cancer Res 66(7):3360–3364

Haglund E, Seale-Goldsmith MM, Leary JF (2009) Design of multifunctional nanomedical systems. Ann Biomed Eng 37(10):2048–2063

Harris JM, Chess RB (2003) Effect of pegylation on pharmaceuticals. Nat Rev Drug Discov 2 (3):214–221

Harris TJ, von Maltzahn G, Lord ME, Park JH, Agrawal A, Min DH et al (2008) Protease-triggered unveiling of bioactive nanoparticles. Small 4(9):1307–1312

Hasebroock KM, Serkova NJ (2009) Toxicity of MRI and CT contrast agents. Expert Opin Drug Metab 5(4):403–416

Heath CH, Deep NL, Sweeny L, Zinn KR, Rosenthal EL (2012) Use of panitumumab-IRDye800 to image microscopic head and neck cancer in an orthotopic surgical model. Ann Surg Oncol 19(12):3879–3887

Hoste K, De Winne K, Schacht E (2004) Polymeric prodrugs. Int J Pharm 277(1–2):119–131

Huang B, Otis J, Joice M, Kotlyar A, Thomas TP (2014) PSMA-targeted stably linked "dendrimer-glutamate urea-methotrexate" as a prostate cancer therapeutic. Biomacromolecules 15(3):915–923

Huynh E, Jin CS, Wilson BC, Zheng G (2014) Aggregate enhanced trimodal porphyrin shell microbubbles for ultrasound, photoacoustic, and fluorescence imaging. Bioconjug Chem 25 (4):796–801

Iyer AK, Khaled G, Fang J, Maeda H (2006) Exploiting the enhanced permeability and retention effect for tumor targeting. Drug Discov Today 11(17–18):812–818

Jang B, Park JY, Tung CH, Kim IH, Choi Y (2011) Gold nanorod-photosensitizer complex for near-infrared fluorescence imaging and photodynamic/photothermal therapy in vivo. ACS Nano 5(2):1086–1094

Janib SM, Moses AS, MacKay JA (2010) Imaging and drug delivery using theranostic nanoparticles. Adv Drug Deliv Rev 62(11):1052–1063

Kaida S, Cabral H, Kumagai M, Kishimura A, Terada Y, Sekino M et al (2010) Visible drug delivery by supramolecular nanocarriers directing to single-platformed diagnosis and therapy of pancreatic tumor model. Cancer Res 70(18):7031–7041

Keereweer S, Kerrebijn JD, van Driel PB, Xie B, Kaijzel EL, Snoeks TJ et al (2011) Optical image-guided surgery—where do we stand? Mol Imaging Biol: MIB 13(2):199–207

Keereweer S, Van Driel PB, Snoeks TJ, Kerrebijn JD, Baatenburg de Jong RJ, Vahrmeijer AL et al (2013) Optical image-guided cancer surgery: challenges and limitations. Clin Cancer Res 19 (14):3745–3754

Kenny GD, Kamaly N, Kalber TL, Brody LP, Sahuri M, Shamsaei E et al (2011) Novel multifunctional nanoparticle mediates siRNA tumour delivery, visualisation and therapeutic tumour reduction in vivo. J Control Release 149(2):111–116

Khandare J, Minko T (2006) Polymer-drug conjugates: progress in polymeric prodrugs. Prog Polym Sci 31(4):359–397

Khlebtsov NG (2008) Optics and biophotonics of nanoparticles with a plasmon resonance. Quantum Electron 38(6):504–529

Khlebtsov N, Bogatyrev V, Dykman L, Khlebtsov B, Staroverov S, Shirokov A et al (2013) Analytical and theranostic applications of gold nanoparticles and multifunctional nanocomposites. Theranostics 3(3):167–180

Kiessling F, Fokong S, Koczera P, Lederle W, Lammers T (2012) Ultrasound microbubbles for molecular diagnosis, therapy, and theranostics. J Nucl Med 53(3):345–348

Klajnert B, Rozanek M, Bryszewska M (2012) Dendrimers in photodynamic therapy. Curr Med Chem 19(29):4903–4912

Konecky SD, Mazhar A, Cuccia D, Durkin AJ, Schotland JC, Tromberg BJ (2009) Quantitative optical tomography of sub-surface heterogeneities using spatially modulated structured light. Opt Express 17(17):14780–14790

Kong G, Braun RD, Dewhirst MW (2000) Hyperthermia enables tumor-specific nanoparticle delivery: effect of particle size. Cancer Res 60(16):4440–4445

Kong G, Braun RD, Dewhirst MW (2001) Characterization of the effect of hyperthermia on nanoparticle extravasation from tumor vasculature. Cancer Res 61(7):3027–3032

Kopecek J, Kopeckova P (2010) HPMA copolymers: origins, early developments, present, and future. Adv Drug Deliv Rev 62(2):122–149

Kulkarni RK, Moore EG, Hegyeli AF, Leonard F (1971) Biodegradable poly(lactic acid) polymers. J Biomed Mater Res 5(3):169–181

Lammers T, Hennink WE, Storm G (2008a) Tumour-targeted nanomedicines: principles and practice. Br J Cancer 99(3):392–397

Lammers T, Subr V, Peschke P, Kuhnlein R, Hennink WE, Ulbrich K et al (2008b) Image-guided and passively tumour-targeted polymeric nanomedicines for radiochemotherapy. Br J Cancer 99(6):900–910

Lammers T, Subr V, Ulbrich K, Peschke P, Huber PE, Hennink WE et al (2009) Simultaneous delivery of doxorubicin and gemcitabine to tumors in vivo using prototypic polymeric drug carriers. Biomaterials 30(20):3466–3475

Lange N (2003) Controlled drug delivery in photodynamic therapy and fluorescence-based diagnosis of cancer. In: Mycek M-A, Pogue BW (eds) Handbook of biomedical fluorescence. Marcel Ekker, New York, pp 563–635

Langereis S, Geelen T, Grull H, Strijkers GJ, Nicolay K (2013) Paramagnetic liposomes for molecular MRI and MRI-guided drug delivery. NMR Biomed 26(7):728–744

Lee GY, Qian WP, Wang LY, Wang YA, Staley CA, Satpathy M et al (2013) Theranostic nanoparticles with controlled release of gemcitabine for targeted therapy and MRI of pancreatic cancer. ACS Nano 7(3):2078–2089

Leproux A, Durkin A, Compton M, Cerussi AE, Gratton E, Tromberg BJ (2013) Assessing tumor contrast in radiographically dense breast tissue using Diffuse Optical Spectroscopic Imaging (DOSI). Breast Cancer Res: BCR 15(5):R89

Li XJ, Takeda K, Yuba E, Harada A, Kono K (2014) Preparation of PEG-modified PAMAM dendrimers having a gold nanorod core and their application to photothermal therapy. J Mater Chem B 2(26):4167–4176

Liu Z, Jiao Y, Wang Y, Zhou C, Zhang Z (2008) Polysaccharides-based nanoparticles as drug delivery systems. Adv Drug Deliv Rev. 60(15):1650–1662

Louie AY (2010) Multimodality imaging probes: design and challenges. Chem Rev 110(5):3146–3195

Luk BT, Zhang L (2014) Current advances in polymer-based nanotheranostics for cancer treatment and diagnosis. ACS Appl Mater Interfaces 21859–21873

Maeda H (2001) SMANCS and polymer-conjugated macromolecular drugs: advantages in cancer chemotherapy. Adv Drug Deliv Rev 46(1–3):169–185

Massoud TF, Gambhir SS (2003) Molecular imaging in living subjects: seeing fundamental biological processes in a new light. Genes Dev 17(5):545–580

Matsumura Y, Maeda H (1986) A new concept for macromolecular therapeutics in cancer chemotherapy: mechanism of tumoritropic accumulation of proteins and the antitumor agent smancs. Cancer Res 46(12 Pt 1):6387–6392

Matsumura Y, Hamaguchi T, Ura T, Muro K, Yamada Y, Shimada Y et al (2004) Phase I clinical trial and pharmacokinetic evaluation of NK911, a micelle-encapsulated doxorubicin. Br J Cancer 91(10):1775–1781

McCarthy JR, Korngold E, Weissleder R, Jaffer FA (2010) A light-activated theranostic nanoagent for targeted macrophage ablation in inflammatory atherosclerosis. Small 6(18):2041–2049

Miele E, Spinelli GP, Miele E, Tomao F, Tomao S (2009) Albumin-bound formulation of paclitaxel (Abraxane ABI-007) in the treatment of breast cancer. Int J Nanomed 4:99–105

Mittra ES, Goris ML, Iagaru AH, Kardan A, Burton L, Berganos R et al (2011) Pilot pharmacokinetic and dosimetric studies of (18)F-FPPRGD2: a PET radiopharmaceutical agent for imaging alpha(v)beta(3) integrin levels. Radiology 260(1):182–191

Modery-Pawlowski CL, Gupta AS (2014) Heteromultivalent ligand-decoration for actively targeted nanomedicine. Biomaterials 35(9):2568–2579

Mok H, Park TG (2012) Hybrid polymeric nanomaterials for siRNA delivery and imaging. Macromol Biosci 12:40–48

Moonen CT (2007) Spatio-temporal control of gene expression and cancer treatment using magnetic resonance imaging-guided focused ultrasound. Clin Cancer Res 13(12):3482–3489

Mulder WJ, Griffioen AW, Strijkers GJ, Cormode DP, Nicolay K, Fayad ZA (2007) Magnetic and fluorescent nanoparticles for multimodality imaging. Nanomedicine 2(3):307–324

Mura S, Couvreur P (2012) Nanotheranostics for personalized medicine. Adv Drug Deliv Rev 64 (13):1394–1416

Muselaers CH, Stillebroer AB, Rijpkema M, Franssen GM, Oosterwijk E, Mulders PF et al (2014) Optical imaging of renal cell carcinoma with anti-carbonic anhydrase IX monoclonal antibody girentuximab. J Nucl Med 55(6):1035–1040

Needham D, Dewhirst MW (2001) The development and testing of a new temperature-sensitive drug delivery system for the treatment of solid tumors. Adv Drug Deliv Rev 53(3):285–305

Needham D, Anyarambhatla G, Kong G, Dewhirst MW (2000) A new temperature-sensitive liposome for use with mild hyperthermia: characterization and testing in a human tumor xenograft model. Cancer Res 60(5):1197–1201

Negussie AH, Yarmolenko PS, Partanen A, Ranjan A, Jacobs G, Woods D et al (2011) Formulation and characterisation of magnetic resonance imageable thermally sensitive liposomes for use with magnetic resonance-guided high intensity focused ultrasound. Int J Hyperth 27(2):140–155

Ng KK, Shakiba M, Huynh E, Weersink RA, Roxin A, Wilson BC et al (2014) Stimuli-responsive photoacoustic nanoswitch for in vivo sensing applications. ACS Nano 8363–8373

Nichols JW, Bae YH (2014) EPR: evidence and fallacy. J Control Release 451–464

Nijssen A, Koljenovic S, Bakker Schut TC, Caspers PJ, Puppels GJ (2009) Towards oncological application of Raman spectroscopy. J Biophotonics 2(1–2):29–36

Nurunnabi M, Cho KJ, Choi JS, Huh KM, Lee YK (2010) Targeted near-IR QDs-loaded micelles for cancer therapy and imaging. Biomaterials 31(20):5436–5444

O'Neal DP, Hirsch LR, Halas NJ, Payne JD, West JL (2004) Photo-thermal tumor ablation in mice using near infrared-absorbing nanoparticles. Cancer Lett 209(2):171–176

Ornelas C, Pennell R, Liebes LF, Weck M (2011) Construction of a well-defined multifunctional dendrimer for theranostics. Org Lett 13(5):976–979

O'Sullivan TD, Leproux A, Chen JH, Bahri S, Matlock A, Roblyer D et al (2013) Optical imaging correlates with magnetic resonance imaging breast density and reveals composition changes during neoadjuvant chemotherapy. Breast Cancer Res: BCR 15(1):R14

Patil YP, Jadhav S (2014) Novel methods for liposome preparation. Chem Phys Lipids 177:8–18

Peer D, Karp JM, Hong S, Farokhzad OC, Margalit R, Langer R (2007) Nanocarriers as an emerging platform for cancer therapy. Nat Nanotechnol 2(12):751–760

Peng CL, Shih YH, Lee PC, Hsieh TM, Luo TY, Shieh MJ (2011) Multimodal image-guided photothermal therapy mediated by 188Re-labeled micelles containing a cyanine-type photosensitizer. ACS Nano 5(7):5594–5607

Petit B, Yan F, Tranquart F, Allemann E (2012a) Microbubbles and ultrasound-mediated thrombolysis: a review of recent in vitro studies. J Drug Deliv Sci Technol 22(5):381–392

Petit B, Gaud E, Colevret D, Arditi M, Yan F, Tranquart F et al (2012b) In vitro sonothrombolysis of human blood clots with BR38 microbubbles. Ultrasound Med Biol 38(7):1222–1233

Ponce AM, Viglianti BL, Yu DH, Yarmolenko PS, Michelich CR, Woo J et al (2007) Magnetic resonance imaging of temperature-sensitive liposome release: drug dose painting and antitumor effects. J Natl Cancer Inst 99(1):53–63

Puri A, Blumenthal R (2011) Polymeric lipid assemblies as novel theranostic tools. Acc Chem Res 44(10):1071–1079

Quan Q, Xie J, Gao H, Yang M, Zhang F, Liu G et al (2011) HSA coated iron oxide nanoparticles as drug delivery vehicles for cancer therapy. Mol Pharm 8(5):1669–1676

Rahmim A, Zaidi H (2008) PET versus SPECT: strengths, limitations and challenges. Nucl Med Commun 29(3):193–207

Ranjan A, Jacobs GC, Woods DL, Negussie AH, Partanen A, Yarmolenko PS et al (2012) Image-guided drug delivery with magnetic resonance guided high intensity focused ultrasound and temperature sensitive liposomes in a rabbit Vx2 tumor model. J Control Release 158 (3):487–494

Redy O, Shabat D (2012) Modular theranostic prodrug based on a FRET-activated self-immolative linker. J Control Release 164(3):276–282

Ringsdorf H (1975) Structure and properties of pharmacologically active polymers. J Polym Sci Polym Symp 51:135–153

Santhosh PB, Ulrih NP (2013) Multifunctional superparamagnetic iron oxide nanoparticles: promising tools in cancer theranostics. Cancer Lett 336(1):8–17

Schwartz JA, Shetty AM, Price RE, Stafford RJ, Wang JC, Uthamanthil RK et al (2009) Feasibility study of particle-assisted laser ablation of brain tumors in orthotopic canine model. Cancer Res 69(4):1659–1667

Sibani SA, McCarron PA, Woolfson AD, Donnelly RF (2008) Photosensitiser delivery for photodynamic therapy. Part 2: systemic carrier platforms. Expert Opin Drug Deliv 5(11):1241–1254

Stillebroer AB, Boerman OC, Desar IM, Boers-Sonderen MJ, van Herpen CM, Langenhuijsen JF et al (2013) Phase 1 radioimmunotherapy study with lutetium 177-labeled anti-carbonic anhydrase IX monoclonal antibody girentuximab in patients with advanced renal cell carcinoma. Eur Urol 64(3):478–485

Straathof R, Strijkers GJ, Nicolay K (2011) Target-specific paramagnetic and superparamagnetic micelles for molecular MR imaging. Methods Mol Biol 771:691–715

Svenson S (2013) Theranostics: are we there yet? Mol Pharm 10(3):848–856

Tagawa ST, Milowsky MI, Morris M, Vallabhajosula S, Christos P, Akhtar NH et al (2013) Phase II study of Lutetium-177-labeled anti-prostate-specific membrane antigen monoclonal antibody J591 for metastatic castration-resistant prostate cancer. Clin Cancer Res 19(18):5182–5191

Talelli M, Rijcken CJ, van Nostrum CF, Storm G, Hennink WE (2010) Micelles based on HPMA copolymers. Adv Drug Deliv Rev 62(2):231–239

Taratula O, Schumann C, Naleway MA, Pang AJ, Chon KJ, Taratula O (2013) A multifunctional theranostic platform based on phthalocyanine-loaded dendrimer for image-guided drug delivery and photodynamic therapy. Mol Pharm 10(10):3946–3958

Teesalu T, Sugahara KN, Ruoslahti E (2013) Tumor-penetrating peptides. Front Oncol 3:216

Tempany CM, Stewart EA, McDannold N, Quade BJ, Jolesz FA, Hynynen K (2003) MR imaging-guided focused ultrasound surgery of uterine leiomyomas: a feasibility study. Radiology 226(3):897–905

Terreno E, Castelli DD, Viale A, Aime S (2010) Challenges for molecular magnetic resonance imaging. Chem Rev 110(5):3019–3042

Terreno E, Uggeri F, Aime S (2012) Image guided therapy: the advent of theranostic agents. J Control Release 161(2):328–337

Thorsen F, Fite B, Mahakian LM, Seo JW, Qin S, Harrison V et al (2013) Multimodal imaging enables early detection and characterization of changes in tumor permeability of brain metastases. J Control Release 172(3):812–822

Topete A, Alatorre-Meda M, Iglesias P, Villar-Alvarez EM, Barbosa S, Costoya JA et al (2014) Fluorescent drug-loaded, polymeric-based, branched gold nanoshells for localized multimodal therapy and imaging of tumoral cells. ACS Nano 8(3):2725–2738

Torchilin VP (2004) Targeted polymeric micelles for delivery of poorly soluble drugs. Cell Mol Life Sci: CMLS 61(19–20):2549–2559

Torchilin VP (2005) Recent advances with liposomes as pharmaceutical carriers. Nat Rev Drug Discov 4(2):145–160

Torchilin VP (2007) Micellar nanocarriers: pharmaceutical perspectives. Pharm Res 24(1):1–16

Torchilin VP, Omelyanenko VG, Papisov MI, Bogdanov AA, Trubetskoy VS, Herron JN et al (1994) Poly(ethylene glycol) on the liposome surface-on the mechanism of polymer-coated liposome longevity. BBA Biomembr 1195(1):11–20

Vahrmeijer AL, Hutteman M, van der Vorst JR, van de Velde CJ, Frangioni JV (2013) Image-guided cancer surgery using near-infrared fluorescence. Nat Rev Clin Oncol 10(9):507–518

van Dam GM, Themelis G, Crane LM, Harlaar NJ, Pleijhuis RG, Kelder W et al (2011) Intraoperative tumor-specific fluorescence imaging in ovarian cancer by folate receptor-alpha targeting: first in-human results. Nat Med 17(10):1315–1319

van Driel PB, van der Vorst JR, Verbeek FP, Oliveira S, Snoeks TJ, Keereweer S et al (2014) Intraoperative fluorescence delineation of head and neck cancer with a fluorescent anti-epidermal growth factor receptor nanobody. Int J Cancer 134(11):2663–2673

Vasey PA, Kaye SB, Morrison R, Twelves C, Wilson P, Duncan R et al (1999) Phase I clinical and pharmacokinetic study of PK1 [N-(2-hydroxypropyl)methacrylamide copolymer doxorubicin]: first member of a new class of chemotherapeutic agents-drug-polymer conjugates. Cancer Research Campaign Phase I/II Committee. Clin Cancer Res 5(1):83–94

Veronese FM, Schiavon O, Pasut G, Mendichi R, Andersson L, Tsirk A et al (2005) PEG-doxorubicin conjugates: influence of polymer structure on drug release, in vitro cytotoxicity, biodistribution, and antitumor activity. Bioconjug Chem 16(4):775–784

Viglianti BL, Abraham SA, Michelich CR, Yarmolenko PS, MacFall JR, Bally MB et al (2004) In vivo monitoring of tissue pharmacokinetics of liposome/drug using MRI: illustration of targeted delivery. Magn Reson Med 51(6):1153–1162

Viglianti BL, Ponce AM, Michelich CR, Yu D, Abraham SA, Sanders L et al (2006) Chemodosimetry of in vivo tumor liposomal drug concentration using MRI. Magn Reson Med 56(5):1011–1018

Wang CY, Ravi S, Martinez GV, Chinnasamy V, Raulji P, Howell M et al (2012) Dual-purpose magnetic micelles for MRI and gene delivery. J Control Release 163(1):82–92

Wang CY, Ravi S, Garapati US, Das M, Howell M, Mallela J et al (2013) Multifunctional chitosan magnetic-graphene (CMG) nanoparticles: a theranostic platform for tumor-targeted co-delivery of drugs, genes and MRI contrast agents. J Mater Chem B 1(35):4396–4405

Weinstein JN, Magin RL, Yatvin MB, Zaharko DS (1979) Liposomes and local hyperthermia: selective delivery of methotrexate to heated tumors. Science 204(4389):188–191

Weishaupt D, Köchli VD, Marincek B (eds) (2006) How does MRI work? An introduction to the physics and function of magnetic resonance imaging. Springer, New York

Weissleder R (1999) Molecular imaging: exploring the next frontier. Radiology 212(3):609–614

Weissleder R (2001) A clearer vision for in vivo imaging. Nat Biotechnol 19(4):316–317

Weissleder R (2002) Scaling down imaging: molecular mapping of cancer in mice. Nat Rev Cancer 2(1):11–18

Wu XM, Sun XR, Guo ZQ, Tang JB, Shen YQ, James TD et al (2014) In vivo and in situ tracking cancer chemotherapy by highly photostable NIR fluorescent theranostic prodrug. J Am Chem Soc 136(9):3579–3588

Xie J, Lee S, Chen XY (2010) Nanoparticle-based theranostic agents. Adv Drug Deliver Rev. 62 (11):1064–1079

Yatvin MB, Weinstein JN, Dennis WH, Blumenthal R (1978) Design of liposomes for enhanced local release of drugs by hyperthermia. Science 202(4374):1290–1293

Yavlovich A, Singh A, Blumenthal R, Puri A (2011) A novel class of photo-triggerable liposomes containing DPPC:DC(8,9)PC as vehicles for delivery of doxorubcin to cells. Biochim Biophys Acta 1808(1):117–126

Yu MK, Jeong YY, Park J, Park S, Kim JW, Min JJ et al (2008) Drug-loaded superparamagnetic iron oxide nanoparticles for combined cancer imaging and therapy in vivo. Angew Chem Int Edit 47(29):5362–5365

Yuan F, Dellian M, Fukumura D, Leunig M, Berk DA, Torchilin VP et al (1995) Vascular-permeability in a human tumor xenograft—molecular-size dependence and cutoff size. Cancer Res 55(17):3752–3756

Zeisser-Labouebe M, Lange N, Gurny R, Delie F (2006) Hypericin-loaded nanoparticles for the photodynamic treatment of ovarian cancer. Int J Pharm 326(1–2):174–181

Zeisser-Labouebe M, Delie F, Gurny R, Lange N (2009) Benefits of nanoencapsulation for the hypercin-mediated photodetection of ovarian micrometastases. Eur J Pharm Biopharm 71 (2):207–213

Zhang Z, Wang J, Chen C (2013) Gold nanorods based platforms for light-mediated theranostics. Theranostics 3(3):223–238

Zuluaga MF, Gabriel D, Lange N (2012) Enhanced prostate cancer targeting by modified protease sensitive photosensitizer prodrugs. Mol Pharm 9(6):1570–1579

Zuluaga MF, Sekkat N, Gabriel D, van den Bergh H, Lange N (2013) Selective photodetection and photodynamic therapy for prostate cancer through targeting of proteolytic activity. Mol Cancer Ther 12(3):306–313